

An Augmented Nonlinear Complex LMS for Digital Self-Interference Cancellation in Full-Duplex Direct-Conversion Transceivers

Zhe Li, *Student Member, IEEE*, Yili Xia, *Member, IEEE*, Wenjiang Pei, Kai Wang, and Danilo P. Mandic, *Fellow, IEEE*

Abstract—In future full-duplex communications, the cancellation of self-interference (SI) arising from hardware nonidealities, will play an important role in the design of mobile-scale devices. To this end, we introduce an optimal digital SI cancellation solution for shared-antenna-based direct-conversion transceivers (DCTs). To establish that the underlying widely linear signal model is not adequate for strong transmit signals, the impacts of various circuit imperfections, including power amplifier (PA) distortion, frequency-dependent I/Q imbalances, quantization noise and thermal noise, on the performance of the conventional augmented complex least mean square (ACLMS) based SI canceller, are analyzed. In order to achieve a sufficient signal-to-noise-plus-interference ratio (SNIR) when the nonlinear SI components are not negligible, we propose an augmented nonlinear CLMS (ANCLMS) based SI canceller for a joint cancellation of both the linear and nonlinear SI components by virtue of a widely-nonlinear model fit. A rigorous mean and mean square performance evaluation is conducted to justify the performance advantages of the proposed scheme over the conventional ACLMS solution. Simulations on orthogonal frequency division multiplexing (OFDM)-based wireless local area network (WLAN) standard compliant waveforms support the analysis.

Index Terms—Full-duplex, I/Q imbalance, self-interference, augmented complex LMS (ACLMS), augmented nonlinear complex LMS (ANCLMS), mean and mean square analysis

I. INTRODUCTION

THE full-duplex (FD) technology aims at doubling the radio link data rate through simultaneous and bidirectional communication at the same center frequency, and is widely considered as a driving-force for more spectrally efficient wireless networks and a potential candidate to fulfill 5G's ambition of a 1000-fold gain in capacity [1], [2]. One of the major challenges in FD communications is the so-called self-interference (SI) problem, a strong transmit signal coupled into the receiver (Rx) path. Since the transmitter (Tx) and

Rx chains are closely linked together in each transceiver node of FD communication systems, the SI power leaked into and reflected from the Tx chain could be even 50 dB to 110 dB higher than the Rx sensitivity level in either wireless local area network (WLAN) or cellular scenarios [3]–[5]. The design of FD transceivers has long been considered impossible for practical realizations and implementations, and it is only recently that its feasibility was experimentally demonstrated using the wireless open-access research platform (WARP) with WiFi waveforms [6]–[11]. Based on this feasibility result, it was recently suggested that a preferable FD network should consist of backhaul nodes operating in the FD mode and access nodes remaining in the legacy half-duplex (HD) mode [12]–[14]. However, recent researcher has showed that operating access nodes in FD mode significantly leverages the gain in degrees of freedom (DoF) in either ergodic or fast-fading channel [15], and an imperative is to design a hardware structure suitable for mass-production. Owing to the small-size, low-cost and low-energy-consumption, direct-conversion transceivers (DCTs) are widely applied in HD wireless systems, and are also suitable for far-end device implementation in the context of FD communication systems.

In order to provide SI cancellation, there exist numerous types of hardware solutions. According to the antenna placement strategies, these can be classified into separate-antennas-based and shared-antenna-based schemes. When each transceiver node is equipped with more than two separate antennas, SI attenuation can be achieved by improving the electromagnetic insulation between the antennas. Owing to the inherent closed-loop of FD systems, the knowledge of the SI channel matrix can be obtained by involving either placing extra transmit antennas or allocating specific spatial resources [16], [17]. On the other hand, the shared-antenna-based design aims to separate the transmit and receive signals by sharing a common antenna [9], [10], the key component of which is a three port routing device, known as a circulator, used to isolate the incoming and outgoing signals. Requiring only off-the-shelf RF components, the shared-antenna structure stands out as a cost-effective and energy-saving choice for the design of mobile-scale FD transceivers, and demonstrations on the WARP have shown that even 110 dB and 103 dB SI cancellation can be respectively achieved in SISO [9] and MIMO systems [10].

In a shared-antenna structure, there is still need for further non-trivial analog and digital SI cancellation, due to the leak-

This work was partially supported by the National Natural Science Foundation of China under Grant 61401094 and Grant 61771124, the Natural Science Foundation of Jiangsu Province under Grant BK20140645, the Fundamental Research Funds for the Central Universities under Grant 2242016K41050, and the China Scholarship Council. (*Corresponding author: Yili Xia.*)

Z. Li is with the School of Information Science and Engineering, Southeast University, 2 Sipailou, Nanjing 210096, P. R. China, and also with the Department of Electrical and Electronic Engineering, Imperial College London, London SW7 2AZ, U.K. (e-mail:lizhe_nanjing@seu.edu.cn)

Y. Xia, W. Pei, and K. Wang are with the School of Information Science and Engineering, Southeast University, 2 Sipailou, Nanjing 210096, P. R. China. (e-mail: yili_xia@seu.edu.cn; wjpei@seu.edu.cn; kaiwang@seu.edu.cn).

D. P. Mandic is with the Department of Electrical and Electronic Engineering, Imperial College London, London SW7 2AZ, U.K. (e-mail: d.mandic@imperial.ac.uk).

age of the circulator, single-path reflection from the antenna, and multi-path interference from the surrounding environment. The purpose of analog SI cancellation is to prevent the saturation of the SI power level of the Rx low-noise amplifier (LNA), and of the same time, to ensure that the difference between the power of residual SI and the received signal of interest does not exceed the dynamic range of an analog-to-digital converter (ADC) [18]. Subsequently, a further digital baseband cancellation is performed to deal with the residual SI components, as well as with RF circuit non-idealities, mainly including nonlinear distortion, I/Q imbalance and phase noise. The nonlinearity is largely caused by the power amplifier (PA), while IQ imbalance and phase noise are mainly induced by the imperfect local oscillator (LO). The impact of PA nonlinear distortion on FD DCTs has been reported and investigated in [19], [20], while the effect of phase noise was analyzed in [21], [22]. Since the I/Q imbalance is essentially reflected in the mismatch between in-phase and quadrature components of the complex-valued I/Q signal, it is reflected in an image interference associated with the original signal [23]–[25].

The impact of the image interference caused by Tx I/Q imbalance on the SI cancellation has been studied in [26], indicating that it heavily limits the receiver path signal-to-noise-plus-interference ratio (SNIR). However, due to size constraints of FD DCTs, the Rx and Tx may share a common imperfect LO, therefore, a more accurate analysis of the impact of image interference on SI cancellation should be performed by a joint consideration of both Tx and Rx I/Q imbalances. Motivated by this finding, a widely linear framework was then developed, whereby not only the original transmit signal, but also its complex conjugate, i.e., the image interference, are jointly processed to form an estimate of the SI signal, followed by block-based parameter estimation methods to estimate the cancellation parameters through widely linear least-squares model fitting [27]. By exploiting the advantages of widely linear adaptive estimation algorithms as compared with block-based ones, such as their lower computational complexity and faster adaptation for potential time-varying channels, the augmented (widely linear) complex least mean square (ACLMS) adaptive filtering algorithm [28]–[30] has been employed in a DSP-assisted analog SI cancellation process, and its theoretical performance in the presence of Tx and Rx IQ imbalances has been evaluated [31]. However, for simplicity, in [31], the I/Q imbalances within transmitters and receivers were considered to be frequency-independent, which is not the case in wideband scenarios, where their frequency selectivity has been extensively reported and justified in [24]. Furthermore, although it has been illustrated by simulations that due to the undermodeling problem, ACLMS yields suboptimal SI cancellation results in the presence of PA nonlinearity, a theoretical understanding of this suboptimality and ways of its mitigation are still lacking.

Therefore, in this paper, we first provide a comprehensive mean and mean square performance analysis of the ACLMS based SI canceller, in both transient and steady-state stages, to theoretically establish its suboptimality in wideband FD DCTs. For rigor, both the PA nonlinear distortion and frequency-dependent image interferences are also considered. Next, in

order to achieve a sufficient amount of SNIR when the nonlinear SI components are not negligible, an augmented nonlinear CLMS (ANCLMS) is proposed for a joint cancellation of both the image and the nonlinear SI components by virtue of a widely-nonlinear model fitting, and a theoretical performance evaluation is conducted to demonstrate its performance advantages over ACLMS. Moreover, to facilitate its use in practical applications, a data pre-whitening scheme is employed to speed up its convergence. Simulations on the proposed canceller with orthogonal frequency division multiplexing (OFDM)-based WLAN standard compliant waveforms applied support the analysis.

Notations: Lowercase letters are used to denote scalars, \mathbf{a} and boldface uppercase letters for column vectors, \mathbf{A} . The superscripts $(\cdot)^*$, $(\cdot)^T$, $(\cdot)^H$ and $(\cdot)^{-1}$ denote respectively the complex conjugation, transpose, Hermitian transpose and matrix inversion operation. The operator $\text{Tr}[\cdot]$ represents the trace of a matrix, while operators \star , \otimes , $\|\cdot\|_2$ respectively denote the convolution, Kronecker product and Frobenius norm. The statistical expectation operator is denoted by $E[\cdot]$, matrix determinant by $\det[\cdot]$, while operators $\Re[\cdot]$ and $\Im[\cdot]$ extract respectively the real and imaginary parts of a complex variable and $j = \sqrt{-1}$. The operator $\text{diag}\{\mathbf{A}\}$ stands for a column vector composed by the diagonal elements of the matrix \mathbf{A} . Matrix vectorization is designated by $\text{vec}\{\cdot\}$, which returns a column vector transformed by stacking the successive columns of matrix, and its inverse operation, i.e., restoring the matrix from the its vectorized form, is denoted by $\text{vec}^{-1}\{\cdot\}$. The extraction of matrix diagonal element into a vector is denoted by $\text{diag}\{\cdot\}$.

II. FULL-DUPLEX TRANSCEIVER AND ITS WIDELY-LINEAR BASEBAND EQUIVALENT MODEL

A. FD DCT

The structure of a typical shared-antenna FD DCT is given in Fig. 1, and due to its simplicity this structure is widely adopted in modern wireless transceivers [32]. We here briefly discuss the physics for I/Q imaging and PA distortion, the two vital impairments within a FD DCT, and we refer to [20] for a complete characterization of the effective SI waveform in different stages of the transceiver.

The I/Q imbalance impairment, characterized by an amplitude difference between the I/Q oscillators, and/or a phase shift from the nominal 90° , is a consequence of the imperfections of I/Q mixers at both the transmitter and receiver chains. In wideband systems, the mismatch between the low-pass filters of the in-phase and quadrature branches also contributes to the frequency selective nature of I/Q imbalance [24], [33]. The Tx frequency-dependent I/Q imbalance process occurs in the red shaded region in Fig. 1, for which input-output relation in discrete-time baseband can be expressed as

$$x_{IQ}(n) = f_{1,T}(n) \star x(n) + f_{2,T}(n) \star x^*(n) \quad (1)$$

where $x(n)$ is the original SI waveform before digital-to-analog-conversion, perfectly known by the receiver, and $x_{IQ}(n)$ is the I/Q imbalanced output of the Tx I/Q mixer. The channel impulse responses (IRs) for the direct signal $x(n)$ and

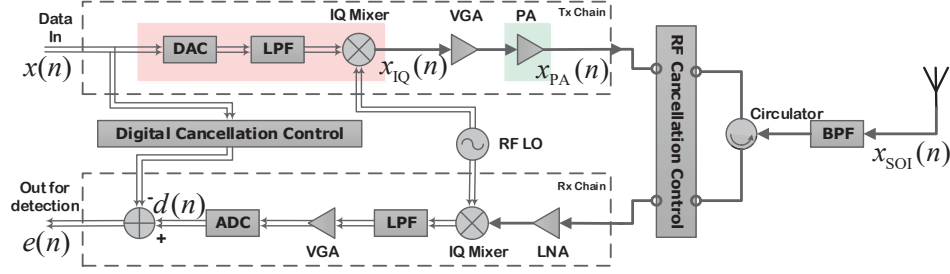


Fig. 1. The architecture of a shared-antenna FD DCT.

TABLE I
NOTATIONS AND SYMBOLS USED.

Symbol	Denotation
$h_{tI}(n)$	Tx frequency-dependent IR of in-phase branch
$h_{tQ}(n)$	Tx frequency-dependent IR of quadrature branch
g_t	Tx frequency-independent gain imbalance
θ_t	Tx frequency-independent phase imbalance
$f_{1,T}(n)$	I/Q imbalance IR of Tx direct component
$f_{2,T}(n)$	I/Q imbalance IR of Tx image component
$f_{1,R}(n)$	I/Q imbalance IR of Rx direct component
$f_{2,R}(n)$	I/Q imbalance IR of Rx image component
k_{IRR}	Image rejection ratio
α_0	PA gain
α_1	Gain of nonlinear PA
k_{BB}	VGA Gain
k_{LNA}	LNA Gain
k_{TIQ}	Tx IQ mixer gain
k_{RIQ}	Rx IQ mixer gain
$v_{th}(n)$	LNA thermal noise
$q(n)$	ADC quantization noise
$f_{PA}(n)$	Memory polynomials of PA
$f_{RFE}(n)$	Estimation error of analog cancellation
p_{sen}	Receiver sensitivity
SNR_{req}	SNR requirement
p_{ADC}	Dynamic range of ADC

its image component $x^*(n)$, that is, $f_{1,T}(n)$ and $f_{2,T}(n)$, can be further described as [24]

$$\begin{aligned} f_{1,T}(n) &= [h_{tI}(n) + g_t e^{-j\theta_t} h_{tQ}(n)]/2 \\ f_{2,T}(n) &= [h_{tI}(n) - g_t e^{-j\theta_t} h_{tQ}(n)]/2 \end{aligned} \quad (2)$$

The physical meaning of $h_{tI}(n)$, $h_{tQ}(n)$, g_t and θ_t are provided in Table I. The type of transformations in (1) and (2), where both the direct and complex-conjugated signals are filtered and finally summed together, are called widely linear [34], [35]. The quality of the I/Q mixer can be quantified by the image rejection ratio (IRR), defined by¹ $k_{IRR} = \|f_{1,T}(n)\|^2 / \|f_{2,T}(n)\|^2$. Note that the I/Q imbalance may also exist in the Rx mixer, and can be characterized in a similar way.

Another considerable impairment within a FD DCT is the PA nonlinearity, which may occur in the green shaded region in Fig. 1. The low-cost PA, which is used in the DCT to enhance the power of a signal before transmission, inevitably causes nonlinear distortion, and the common approach to describe its wideband behavior is via the Wiener-Hammerstein model, given by [36]

$$x_{PA}(n) = f_{PA}(n) \star [\alpha_0 x_{IQ}(n) + \alpha_1 |x_{IQ}(n)|^2 x_{IQ}(n)] \quad (3)$$

¹In fact, the IRR is frequency-dependent in wideband transceivers, and here a constant is used to represent the averaged IRR over the whole spectrum.

The physical meanings for α_0 , α_1 and $f_{PA}(n)$ in (3) are provided in Table I. Note that the gain from Tx variable gain amplifier (VGA) is omitted, since it is linear and can be absorbed into the SI waveform $x(n)$. The nonlinear term on the right hand side (RHS) of (3) is the third-order intermodulation term, which is much stronger compared with other terms beyond third-order. For simplicity, we shall now omit the descriptions of other modules within the FD DCT in Fig. 1, as well as other less significant impairments, such as phase noise and timing error, to yield a simplified widely linear relation from the SI waveform $x(n)$ in the transmitter to the digitalized signal $d(n)$ in the receiver, given by [20]

$$d(n) = h(n) \star x(n) + g(n) \star x^*(n) + x_{SOI}(n) + u(n) \quad (4)$$

where $h(n)$ and $g(n)$ are the end-to-end channel IRs for the direct component $x(n)$ and its image counterpart $x^*(n)$, given by

$$\begin{aligned} h(n) &= \alpha_0 \sqrt{k_{BB} k_{LNA}} \{f_{1,R}(n) \star f_{1,T}(n) \star f_{PA}(n) \star f_{RFE}(n) \\ &\quad + f_{2,R}(n) \star f_{2,T}^*(n) \star f_{PA}^*(n) \star f_{RFE}^*(n)\} \\ &\approx \alpha_0 \sqrt{k_{BB} k_{LNA}} f_{1,R}(n) \star f_{1,T}(n) \star f_{PA}(n) \star f_{RFE}(n) \end{aligned} \quad (5)$$

$$\begin{aligned} g(n) &= \alpha_0 \sqrt{k_{BB} k_{LNA}} \{f_{1,R}(n) \star f_{2,T}(n) \star f_{PA}(n) \star f_{RFE}(n) \\ &\quad + f_{2,R}(n) \star f_{1,T}^*(n) \star f_{PA}^*(n) \star f_{RFE}^*(n)\} \end{aligned} \quad (6)$$

The physical meanings of α_0 , $f_{1,R}(n)$, $f_{2,R}(n)$ and $f_{RFE}(n)$ are listed in Table I. Suppose that Tx and Rx mixers have the same level of IRR at k_{IRR} dB, then, from (5) and (6), we observe that the second term on the RHS of (5) is negligible, since it is $20 \log k_{IRR}$ dB weaker than the first one, and the power of $g(n)$ is considered to be $(10 \log k_{IRR} - 3)$ dB lower than that of $h(n)$. The third term on the RHS of (4), that is, $x_{SOI}(n)$, is the received signal of interest, whose power before the digital SI cancellation can be calculated as

$$p_{x_{SOI}} = p_{sen} k_{LNA} k_{BB} k_{RIQ} \quad (7)$$

where k_{RIQ} is the Rx mixer gain, defined as $k_{RIQ} = \|f_{1,R}(n)\|^2$. The explanations for the other parameters can be also found in Table I. The composite noise term, that is, $u(n)$ in (4), represents the sum of interference components, including PA nonlinearity, thermal noise and quantization noise from an ADC, given by [20]

$$\begin{aligned} u(n) &= h_{IMD}(n) \star x_{IMD}(n) + g_{IMD}(n) \star x_{IMD}^*(n) \\ &\quad + v(n) + v_{IMG}(n) + q(n) \end{aligned} \quad (8)$$

where

$$x_{\text{IMD}}(n) = |x_{\text{IQ}}(n)|^2 x_{\text{IQ}}(n) \approx k_{\text{TIQ}}^{3/2} |x(n)|^2 x(n) \quad (9)$$

$$h_{\text{IMD}}(n) = \alpha_1 \sqrt{k_{\text{BB}} k_{\text{LNA}}} f_{1,\text{R}}(n) \star f_{\text{PA}}(n) \star f_{\text{RFE}}(n) \quad (10)$$

$$g_{\text{IMD}}(n) = \alpha_1 \sqrt{k_{\text{BB}} k_{\text{LNA}}} f_{2,\text{R}}(n) \star f_{\text{PA}}^*(n) \star f_{\text{RFE}}^*(n) \quad (11)$$

$$v(n) = \sqrt{k_{\text{BB}} k_{\text{LNA}}} f_{1,\text{R}}(n) \star v_{\text{th}}(n) \quad (12)$$

$$v_{\text{IMG}}(n) = \sqrt{k_{\text{BB}} k_{\text{LNA}}} f_{2,\text{R}}(n) \star v_{\text{th}}^*(n) \quad (13)$$

in which, $x_{\text{IMD}}(n)$ represents the third-order intermodulated (IMD) component in (3), and $k_{\text{TIQ}} = \|f_{1,\text{T}}(n)\|^2$ is the Tx mixer gain. The approximation in (9) is made by considering a realistic situation for typical FD I/Q imbalance parameters, whereby the energy of the signal output from the Tx mixer is mainly concentrated in the light-of-sight path [33]. The corresponding channel IRs for $x_{\text{IMD}}(n)$ and its image counterpart $x_{\text{IMD}}^*(n)$ are denoted respectively by $h_{\text{IMD}}(n)$ and $g_{\text{IMD}}(n)$. The interference, resulted from thermal noise during the digital SI cancellation process, is represented by $v(n)$ in (12), where $v_{\text{th}}(n)$ denotes the thermal noise induced by a LNA, and $v_{\text{IMG}}(n)$ in (13) is an image counterpart of $v(n)$. The quantization noise is denoted by $q(n)$, whose power is subject to the number of ADC bits and the peak-to-average-power-ratio (PAPR) of $d(n)$.

B. Widely-linear Modelling in a Vectorized Form and Signal Assumptions

For mathematical simplicity, we consider a vectorized form to represent the widely linear relation between the observed signal $d(n)$ and its corresponding SI waveform $x(n)$ in (4), given by

$$d(n) = \mathbf{x}^T(n) \mathbf{h}^o + \mathbf{x}^H(n) \mathbf{g}^o + u(n) \quad (14)$$

where $\mathbf{h}^o = [h_1^o, \dots, h_M^o]^T$ and $\mathbf{g}^o = [g_1^o, \dots, g_M^o]^T$ are the optimal end-to-end channel IRs, determined by transmit and receive frequency-dependent I/Q imbalances, PA memory and residual of analog cancellation, as given in (5) and (6). $\mathbf{x}(n) = [x(n), x(n-1), \dots, x(n-M+1)]^T$ is of length M , whereby the SI waveform $x(n)$ is a zero-mean proper white Gaussian random variable with variance σ_x^2 . The Gaussianity and properness assumptions on $x(n)$ are valid for wideband OFDM waveforms. Indeed, the work in [37] verified that a bandlimited uncoded OFDM symbol converges to a proper Gaussian random process as the number of subcarriers increases, and its whiteness is guaranteed due to the fact that $x(n)$ is independent temporally. The analysis in [27] illustrates that under practical conditions, the power of the image thermal noise signal $v_{\text{IMG}}(n)$ is much lower than those of the other components. Therefore, based on (8), the expression for the overall noise signal $u(n)$ can be simplified as

$$u(n) = \mathbf{x}_{\text{IMD}}^T(n) \mathbf{h}_{\text{IMD}}^o + \mathbf{x}_{\text{IMD}}^H(n) \mathbf{g}_{\text{IMD}}^o + v(n) + q(n) \quad (15)$$

in which $\mathbf{h}_{\text{IMD}}^o = [h_{\text{IMD},1}^o, h_{\text{IMD},2}^o, \dots, h_{\text{IMD},N}^o]^T$ and $\mathbf{g}_{\text{IMD}}^o = [g_{\text{IMD},1}^o, g_{\text{IMD},2}^o, \dots, g_{\text{IMD},N}^o]^T$ with $N < M$ respectively represent the end-to-end channel IRs of the IMD SI components, that is, $\mathbf{x}_{\text{IMD}}(n) = [x_{\text{IMD}}(n), x_{\text{IMD}}(n-1), \dots, x_{\text{IMD}}(n-N+1)]^T$, and

its complex conjugate $\mathbf{x}_{\text{IMD}}^*(n)$. Then, from (9), we know that $x_{\text{IMD}}(n)$ is a zero-mean complex-valued random variable, whose variance $\sigma_{x_{\text{IMD}}}^2$ is given by

$$\sigma_{x_{\text{IMD}}}^2 = E[|x_{\text{IMD}}(n)|^2] = 6k_{\text{TIQ}}^3 \sigma_x^6 \quad (16)$$

By assuming that $v_{\text{th}}(n)$ is a zero-mean complex-valued additive white Gaussian noise (AWGN), its variance $\sigma_{v_{\text{th}}}^2$ can be determined as

$$\sigma_{v_{\text{th}}}^2 = \frac{p_{\text{sen}}}{\text{SNR}_{\text{req}}} \quad (17)$$

where p_{sen} is the sensitivity level of the receiver and SNR_{req} is the SNR requirement, and hence, from (12), the AWGN nature of $v(n)$ can be also guaranteed, and its variance σ_v^2 can be obtained as

$$\sigma_v^2 = E[|v(n)|^2] = k_{\text{BB}} k_{\text{LNA}} k_{\text{RIQ}} \sigma_{v_{\text{th}}}^2 = \frac{k_{\text{BB}} k_{\text{LNA}} k_{\text{RIQ}} p_{\text{sen}}}{\text{SNR}_{\text{req}}} \quad (18)$$

The quantization noise $q(n)$ is assumed to be another zero-mean AWGN process with variance σ_q^2 , and is independent of $v(n)$. In this way, the VGA gain k_{BB} , used to ensure the received signal fit within the voltage range of the ADC, can be calculated as

$$k_{\text{BB}} = \frac{p_{\text{ADC}}}{k_{\text{LNA}} k_{\text{RIQ}} ([\alpha_0^2 k_{\text{TIQ}} \sigma_x^2 + 6\alpha_1^2 k_{\text{TIQ}}^3 \sigma_x^6] \|f_{\text{RFE}}(n)\|_2^2 + p_{\text{sen}})} \quad (19)$$

where p_{ADC} is the dynamic range of the ADC.

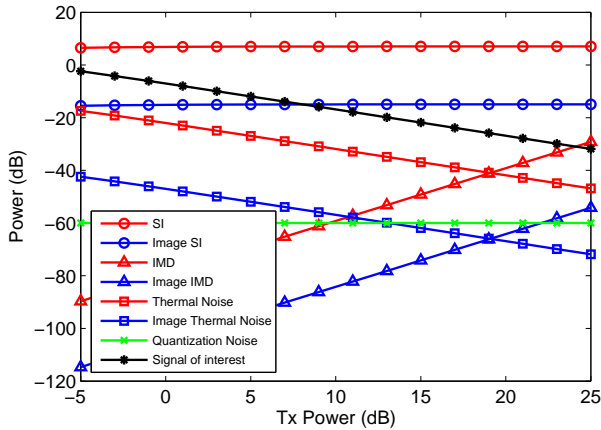
C. Component Analysis

From (4), observe that in a possible FD DCT, the baseband signal before digital SI cancellation is composed of various interference components, including SI $\mathbf{x}(n)$, IMD SI $\mathbf{x}_{\text{IMD}}(n)$, thermal noise $v(n)$ and their image counterparts, as well as quantization noise $q(n)$. In order to visualize which terms are counted as primary interferences, simulations were carried out to illustrate their relative powers within FD DCTs. Typical system parameters, as suggested by [27], were chosen, and they are listed in Table II, which shows that two types of FD DCTs with practical levels of analog SI cancellation are considered. The Type 2 DCT exhibits an inferior analog SI cancellation capability than its Type 1 counterpart, resulting in a weaker received signal of interest and thermal noise. The power of the thermal noise was chosen to be 15 dB below the receiver sensitivity, while that of the received signal of interest at the input of the receiver chain was exactly at the sensitivity level, as defined in (7). The impact of the analog cancellation on the DCT is indicated by the power of the analog cancellation error vector $f_{\text{RFE}}(n)$, which is incorporated into the channel IRs \mathbf{h}^o , \mathbf{g}^o , $\mathbf{h}_{\text{IMD}}^o$ and $\mathbf{g}_{\text{IMD}}^o$. The coefficients of the filters are given to ensure the mixer gain k_{TIQ} or k_{RIQ} is 6 dB and IRR level is 25 dB, a specific requirement of 3GPP LTE [38]. The PA input-referred third-order intercept point (IIP3), represented by α_0/α_1 , is a fictitious point used to determine the power level of the third-order nonlinear distortion in the Tx output.

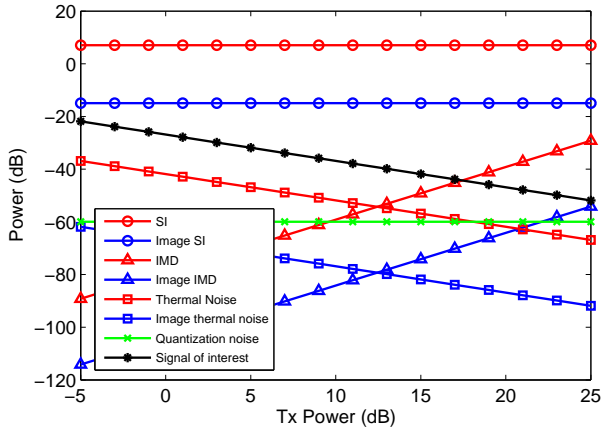
As shown in Fig. 2(a), in a Type 1 FD DCT, the SI component $\mathbf{x}(n)$ and its image counterpart $\mathbf{x}^*(n)$ were both

TABLE II
SYSTEM PARAMETERS OF TYPICAL FD DCTs

Parameter	Value	Notation
Receiver Sensitivity	-89 dBm	p_{sen}
SNR requirement	15 dB	SNR_{req}
Thermal noise floor	-104 dBm	$\sigma_{v_{th}}^2$
RF separation	40 dB (Type 1) 30 dB (Type 2)	$\frac{\ h_0\ ^2}{k_{TIQ}k_{RIQ}}$
RF attenuation	30 dB (Type 1) 20 dB (Type 2)	
IRR	25 dB	k_{IRR}
Tx mixer gain	6 dB	k_{TIQ}
Rx mixer gain	6 dB	k_{RIQ}
PA gain	27 dB	α_0^2
PA IIP3	20 dBm	α_0/α_1
LNA gain	25 dB	k_{LNA}
Transmit power	-5 ~ 25 dB	$\sigma_x^2 \alpha_0^2 k_{TIQ}$
ADC dynamic range	7 dB	p_{ADC}
Quantization noise power	-60 dBm	σ_q^2



(a) Type 1



(b) Type 2

Fig. 2. The power comparison among different signal components in representative FD DCTs, before digital SI cancellation and against different levels of transmit powers. (a) Type 1. (b) Type 2.

the dominant interferences to the signal of interest in the entire transmit power range, and when the transmit power becomes higher, the IMD SI component $\mathbf{x}_{IMD}(n)$ linearly increases to be another major interference. On the other hand, as indicated by Fig. 2(b), in a Type 2 FD DCT, when the transmit power

goes above 20 dBm, the thermal noise $v(n)$ would become weaker than the quantization noise $q(n)$ and the image IMD SI $\mathbf{x}_{IMD}^*(n)$. This is because either a stronger nonlinear SI or a less efficient analog cancellation results in a lower VGA gain, which in turn yields a weaker amplification of signal of interest $x_{SOI}(n)$ and thermal noise $v(n)$, as indicated by (7), (17) and (19).

III. CONVENTIONAL ACLMS BASED SI CANCELLER AND ITS PERFORMANCE ANALYSIS

As discussed in Section II, the effect of Tx and Rx IQ imbalances is to make both the SI component and its image counterpart the dominant interferences in a FD DCT. To mitigate this issue, a widely linear model based augmented complex least mean square (ACLMS) adaptive filtering algorithm was employed in [31] as a further DSP-assisted canceller after the analog SI cancellation procedure, and a preliminary SI cancellation performance analysis of ACLMS was conducted. For simplicity, the I/Q imbalances within transmitter and receiver were considered to be frequency-independent in [31], which, however, is not the case in wideband scenarios, where frequency selectivity has been rigorously justified [24]. Furthermore, it has been illustrated by simulations that ACLMS yields suboptimal SI cancellation results in the presence of PA nonlinearity, since it arbitrarily excludes the nonlinear SI components from its underlying observation model, which in fact can be outstanding among all the imperfections, as shown in Section II-C. Meanwhile, a theoretical quantification of this suboptimality is still missing. Therefore, in this section, we provide a comprehensive mean and mean square convergence analysis of the conventional ACLMS based SI canceller in the presence of both frequency-dependent Tx and Rx I/Q imbalances and PA nonlinear distortion. A unified statistical framework to quantify the SI cancellation performance of ACLMS in both transient and steady-state stages is investigated. For rigor, the proposed analysis covers both the cases of low and high transmit powers. For the compactness of analysis, we first represent the widely linear model in (14) in an augmented form, given by

$$d(n) = \mathbf{x}^a(n) \mathbf{w}^{ao} + u(n) \quad (20)$$

where $\mathbf{x}^a(n) = [\mathbf{x}^T(n), \mathbf{x}^H(n)]^T$ is the $2M \times 1$ augmented SI vector, and $\mathbf{w}^{ao} = [\mathbf{h}^{oT}, \mathbf{g}^{oT}]^T$ is the augmented optimal end-to-end system IRs, which model the transmit and receive frequency-dependent I/Q imbalances, PA distortion and the residual of analog SI cancellation.

The ACLMS estimates the set of system parameters \mathbf{w}^{ao} by minimising the MSE cost function $J^a(n)$, defined as [28]–[30]

$$J^a(n) = E[|e^a(n)|^2] = E[e^a(n)e^{a*}(n)] \quad (21)$$

where $e^a(n)$ is the instantaneous output error, given by

$$e^a(n) = d(n) - \mathbf{x}^a(n) \mathbf{w}^a(n) \quad (22)$$

in which the augmented weight vector of ACLMS, that is, $\mathbf{w}^a(n)$, is updated as

$$\mathbf{w}^a(n+1) = \mathbf{w}^a(n) + \mu e^a(n) \mathbf{x}^{a*}(n) \quad (23)$$

where μ is the step size [28], [39].

A. Mean Convergence Analysis

Upon introducing the $2M \times 1$ weight error vector

$$\tilde{\mathbf{w}}^a(n) = \mathbf{w}^a(n) - \mathbf{w}^{ao} \quad (24)$$

the filter output $e^a(n)$ in (22) becomes

$$e^a(n) = u(n) - \mathbf{x}^{aT}(n)\tilde{\mathbf{w}}^a(n) \quad (25)$$

From (23), the recursion for the update of the weight error vector $\tilde{\mathbf{w}}^a(n)$ can be derived as

$$\tilde{\mathbf{w}}^a(n+1) = [\mathbf{I}_{2M} - \mu \mathbf{x}^{a*}(n) \mathbf{x}^{aT}(n)] \tilde{\mathbf{w}}^a(n) + \mu u(n) \mathbf{x}^{a*}(n) \quad (26)$$

where \mathbf{I}_{2M} is an $2M \times 2M$ identity matrix.

The mean behavior of $\tilde{\mathbf{w}}^a(n)$ can now be determined by applying the statistical expectation operator $E[\cdot]$ to both sides of (26) and upon employing the standard independence assumptions [40]–[45], that is, the composite noise $u(n)$ is statistically independent of any other signal in ACLMS, and $\tilde{\mathbf{w}}^a(n)$ is statistically independent of the augmented SI input vector $\mathbf{x}^{aT}(n)$, to yield

$$E[\tilde{\mathbf{w}}^a(n+1)] = [\mathbf{I}_{2M} - \mu \mathbf{R}^a] E[\tilde{\mathbf{w}}^a(n)] + \mu E[u(n) \mathbf{x}^{a*}(n)] \quad (27)$$

where \mathbf{R}^a is the covariance matrix of the augmented SI vector $\mathbf{x}^a(n)$, defined as

$$\mathbf{R}^a = E[\mathbf{x}^a(n) \mathbf{x}^{aH}(n)] = \sigma_x^2 \mathbf{I}_{2M} \quad (28)$$

Therefore, the convergence of ACLMS in the mean is guaranteed if the step-size μ satisfies [44]

$$0 < \mu < \frac{2}{\lambda_{\max}[\mathbf{R}^a]} = \frac{2}{\sigma_x^2} \quad (29)$$

From Fig. 2(a) and Fig. 2(b) in Section II-C, we observe that the relative power relationships among different SI components vary as the transmit power changes. Therefore, in order to accurately describe the statistical mean behaviour of the ACLMS based SI canceller, we next consider two case studies as

1) *Low transmit power:* When the transmit power is low, both the nonlinear distortion component $\mathbf{x}_{\text{IMD}}(n)$ and the quantization noise $q(n)$ at the receiver are negligible, since their powers are much weaker than that of the thermal noise $v(n)$ in (15). Therefore, from (20), we have $u(n) \simeq v(n)$ and hence, at the steady-state, i.e., $n \rightarrow \infty$, from (27)

$$E[\tilde{\mathbf{w}}^a(\infty)] = \mathbf{0} \quad (30)$$

2) *High transmit power:* When the transmit power is high, the nonlinear PA distortion component $\mathbf{x}_{\text{IMD}}(n)$ becomes the third strongest interference among all the imperfections considered. Upon using the independence assumptions and (15), the second term on the RHS of (27) can be derived as

$$\begin{aligned} E[u(n) \mathbf{x}^{a*}(n)] &= E[(\mathbf{x}_{\text{IMD}}^T(n) \mathbf{h}_{\text{IMD}}^0 + \mathbf{x}_{\text{IMD}}^H(n) \mathbf{g}_{\text{IMD}}^0) \mathbf{x}^{a*}(n)] \\ &= k_{\text{TIQ}}^{3/2} \left\{ \sum_{i=1}^N E[h_{\text{IMD},i} |x(n-i+1)|^2 x(n-i+1) \mathbf{x}^{a*}(n)] \right. \\ &\quad \left. + \sum_{i=1}^N E[g_{\text{IMD},i} |x(n-i+1)|^2 x^*(n-i+1) \mathbf{x}^{a*}(n)] \right\} \\ &= k_{\text{TIQ}}^{3/2} E[|x(n)|^4] [\mathbf{h}_{\text{IMD}}^{oT}, \mathbf{0}_{M-N}^T, \mathbf{g}_{\text{IMD}}^{oT}, \mathbf{0}_{M-N}^T]^T \\ &= 2k_{\text{TIQ}}^{3/2} \sigma_x^4 [\mathbf{h}_{\text{IMD}}^{oT}, \mathbf{0}_{M-N}^T, \mathbf{g}_{\text{IMD}}^{oT}, \mathbf{0}_{M-N}^T]^T \end{aligned} \quad (31)$$

where $\mathbf{0}_{M-N}$ represents an $(M-N) \times 1$ zero vector. The last step is performed by using the Gaussian fourth order moment factorizing theorem and since $x(n)$ is proper, we have $E[|x(n)|^4] = 2\sigma_x^4$ [40]–[43]. From (27), the steady-state value of the weight error vector, that is, $E[\tilde{\mathbf{w}}^a(\infty)]$, can be evaluated as

$$\begin{aligned} E[\tilde{\mathbf{w}}^a(\infty)] &= (\mathbf{R}^{a*})^{-1} E[u(n) \mathbf{x}^{a*}(n)] \\ &= 2k_{\text{TIQ}}^{3/2} \sigma_x^2 [\mathbf{h}_{\text{IMD}}^{oT}, \mathbf{0}_{M-N}^T, \mathbf{g}_{\text{IMD}}^{oT}, \mathbf{0}_{M-N}^T]^T \end{aligned} \quad (32)$$

Remark 1: The upper bound on the step size μ for the mean convergence of ACLMS for a low transmit power FD DCT is identical to that for a high transmit power one. At the steady state, when the transmit power is low, ACLMS converges in the mean to the optimal weight coefficients associated with $\mathbf{x}^a(n)$, that is, \mathbf{w}^{ao} in (20), in an unbiased manner. However, as indicated by (32), when the transmit power is high, this yields a bias in the estimation of $2N$ out of $2M$ entries of the weight error vector $E[\tilde{\mathbf{w}}^a(\infty)]$, quantified by $2k_{\text{TIQ}}^{3/2} \sigma_x^2 [\mathbf{h}_{\text{IMD}}^{oT}, \mathbf{g}_{\text{IMD}}^{oT}]^T$. The level of this bias depends upon the level of undermodeling, that is, the transmitter mixer gain k_{TIQ} , the transmit SI signal power σ_x^2 , and the channel IRs associated with the IMD SI components, that is, $\mathbf{h}_{\text{IMD}}^0$ and $\mathbf{g}_{\text{IMD}}^0$, whose values are determined by receiver frequency-dependent I/Q imbalances, PA memory and residual of analog SI cancellation, as shown in (10) and (11).

B. Mean-Square Convergence Analysis

From (21) and (25), and again by employing the standard independence assumptions stated in Section III-A, the MSE of ACLMS based SI canceller, that is, $J^a(n)$, can be further evaluated as

$$\begin{aligned} J^a(n) &= E[\tilde{\mathbf{w}}^{aH}(n) \mathbf{x}^{a*}(n) \mathbf{x}^{aT}(n) \tilde{\mathbf{w}}^a(n)] + E[|u(n)|^2] \\ &\quad - E[u^*(n) \mathbf{x}^{aT}(n) \tilde{\mathbf{w}}^a(n)] - E[u(n) \tilde{\mathbf{w}}^{aH}(n) \mathbf{x}^{a*}(n)] \\ &= \text{Tr}[\mathbf{R}^{a*} \mathbf{K}^a(n)] + E[|u(n)|^2] - E[u^*(n) \mathbf{x}^{aT}(n)] E[\tilde{\mathbf{w}}^a(n)] \\ &\quad - E[u(n) \mathbf{x}^{aH}(n)] E[\tilde{\mathbf{w}}^{a*}(n)] \end{aligned} \quad (33)$$

where $\mathbf{K}^a(n) = E[\tilde{\mathbf{w}}^a(n) \tilde{\mathbf{w}}^{aH}(n)]$ is the covariance matrix of the augmented weight error vector $\tilde{\mathbf{w}}^a(n)$. It can be observed from (33) that the mean square convergence analysis of ACLMS now rests upon both the first and second order statistical properties of $\tilde{\mathbf{w}}^a(n)$. To this end, we first apply the Hermitian operator $(\cdot)^H$ to both sides of (26), to yield

$$\tilde{\mathbf{w}}^{aH}(n+1) = \tilde{\mathbf{w}}^{aH}(n) [\mathbf{I}_{2M} - \mu \mathbf{x}^{a*}(n) \mathbf{x}^{aT}(n)] + \mu u^*(n) \mathbf{x}^{aT}(n) \quad (34)$$

Upon multiplying (34) to both sides of (26) with (34) and taking the statistical expectation $E[\cdot]$, the evolution of the weight error covariance matrix $\mathbf{K}^a(n)$ now becomes

$$\begin{aligned} \mathbf{K}^a(n+1) &= (1 - 2\mu\sigma_x^2) \mathbf{K}^a(n) + 2\mu \Re[\mathbf{Q}_3(n)] \\ &\quad + \mu^2 [\mathbf{Q}_1(n) + \mathbf{Q}_2(n) - \mathbf{Q}_4(n) - \mathbf{Q}_5(n)] \end{aligned} \quad (35)$$

where

$$\begin{aligned} \mathbf{Q}_1(n) &= E[|u(n)|^2 \mathbf{x}^{a*}(n) \mathbf{x}^{aT}(n)] \\ \mathbf{Q}_2(n) &= E[\mathbf{x}^{a*}(n) \mathbf{x}^{aT}(n) \tilde{\mathbf{w}}^a(n) \tilde{\mathbf{w}}^{aH}(n) \mathbf{x}^{a*}(n) \mathbf{x}^{aT}(n)] \\ \mathbf{Q}_3(n) &= E[u(n) \mathbf{x}^{a*}(n)] E[\tilde{\mathbf{w}}^{aH}(n)] \\ \mathbf{Q}_4(n) &= E[u(n) \mathbf{x}^{a*}(n) \mathbf{x}^{aH}(n) \mathbf{x}^{a*}(n)] E[\tilde{\mathbf{w}}^{aT}(n)] \\ \mathbf{Q}_5(n) &= E[u^*(n) \mathbf{x}^{a*}(n) \mathbf{x}^{aT}(n) \mathbf{x}^a(n)] E[\tilde{\mathbf{w}}^a(n)] \end{aligned} \quad (36)$$

It can be observed that $\mathbf{Q}_2(n)$ is independent from the IMD component $\mathbf{x}_{\text{IMD}}(n)$, and hence [41]–[43]

$$\mathbf{Q}_2(n) = \sigma_x^4 \mathbf{K}^a(n) + \mathbf{P}^{a*} \mathbf{K}^{aT}(n) \mathbf{P}_a + 2M\sigma_x^4 \mathbf{I}_{2M} \text{Tr}[\mathbf{K}^a(n)] \quad (37)$$

where \mathbf{P}^a is the pseudocovariance matrix of the augmented SI vector $\mathbf{x}^a(n)$, given by

$$\mathbf{P}^a = E[\mathbf{x}^a(n) \mathbf{x}^{aT}(n)] = \begin{bmatrix} \mathbf{0} & \sigma_x^2 \mathbf{I}_M \\ \sigma_x^2 \mathbf{I}_M & \mathbf{0} \end{bmatrix}$$

in which \mathbf{I}_M is an $M \times M$ identity matrix. The term $\text{Tr}[\mathbf{K}^a(n)]$ on the RHS of (37) can be decomposed as $\mathbf{1}_{2M}^T \boldsymbol{\kappa}^a(n)$, where $\boldsymbol{\kappa}^a(n)$ is a $2M \times 1$ vector, whose entries are the diagonal elements of $\mathbf{K}^a(n)$, defined as

$$\boldsymbol{\kappa}^a(n) = [E[|\tilde{w}_1^a(n)|^2], E[|\tilde{w}_2^a(n)|^2], \dots, E[|\tilde{w}_{2M}^a(n)|^2]]^T \quad (38)$$

and $\mathbf{1}_{2M}$ denotes a $2M \times 1$ vector in which all the entries are unities. Then, based on (35), the evolution of $\boldsymbol{\kappa}^a(n)$ becomes

$$\begin{aligned} \boldsymbol{\kappa}^a(n+1) &= \underbrace{\{\mathbf{I}_{2M} - 2\mu\sigma_x^2 \mathbf{I}_{2M} + 2\mu^2\sigma_x^4 \mathbf{I}_{2M} + \mu^2\sigma_x^4 \mathbf{1}_{2M} \mathbf{1}_{2M}^T\}}_{\mathbf{F}^a} \boldsymbol{\kappa}^a(n) \\ &\quad + 2\mu \text{diag}\{\Re[\mathbf{Q}_3(n)]\} + \mu^2 \text{diag}\{\mathbf{Q}_1(n) - \mathbf{Q}_4(n) - \mathbf{Q}_5(n)\} \end{aligned} \quad (39)$$

The convergence of the recursion for the vector $\boldsymbol{\kappa}^a(n)$ in (39) is subject to two conditions: 1) the terms $\mathbf{Q}_1(n)$, $\mathbf{Q}_3(n)$, $\mathbf{Q}_4(n)$ and $\mathbf{Q}_5(n)$ are bounded, which is guaranteed if $E[\tilde{\mathbf{w}}^a(n)]$ is bounded; 2) all the eigenvalues of the transition matrix \mathbf{F}^a are less than unity [46]. From (29), Condition 1) holds when $0 < \mu < 2/\sigma_x^2$. Furthermore, the eigenvalues of \mathbf{F}^a , denoted by λ_i^a , where $i = 1, 2, \dots, 2M$, can be obtained by solving $\det[\mathbf{F}^a - \lambda_i^a \mathbf{I}_{2M}] = 0$, and from (39), it is easy to find that \mathbf{F}^a is Toeplitz, for which the diagonal elements are $1 - 2\mu + 3\mu^2\sigma_x^4$, and off-diagonal ones are $\mu^2\sigma_x^4$. Hence, after a few manipulations, we have

$$\lambda_1^a = 1 - \mu\sigma_x^2 + (2M + 2)\mu^2\sigma_x^4 \quad (40)$$

$$\lambda_j^a = 1 - \mu\sigma_x^2 + 2\mu^2\sigma_x^4, \quad j = 2, 3, \dots, 2M \quad (41)$$

Note that since $M \geq 1$, we have $\lambda_1^a > \lambda_j^a$, and hence, Condition 2) is satisfied if $\lambda_1^a < 1$, to yield

$$0 < \mu < \frac{1}{(M+1)\sigma_x^2} \quad (42)$$

Remark 2: The upper bound in (42) is tighter than that in Condition 1), and therefore, the mean square convergence of ACLMS based SI canceller in the presence of frequency-dependent IQ imbalances and PA distortion is guaranteed if the step-size μ satisfies (42).

C. Steady State Analysis

Suppose that step-size μ is chosen such that the mean square stability of ACLMS is guaranteed [47]. Consider $n \rightarrow \infty$ and based on (33) and (38), its steady-state MSE $J^a(\infty)$ can be expressed as

$$J^a(\infty) = \sigma_x^2 \mathbf{1}_{2M}^T \boldsymbol{\kappa}^a(\infty) + E[|u(\infty)|^2] - 2\text{Tr}\{\Re[\mathbf{Q}_3(\infty)]\} \quad (43)$$

where, based on (39), $\boldsymbol{\kappa}^a(\infty)$ can be derived as

$$\begin{aligned} \boldsymbol{\kappa}^a(\infty) &= 2\mu(\mathbf{I}_{2M} - \mathbf{F}^a)^{-1} [\text{diag}\{\Re[\mathbf{Q}_3(\infty)]\} \\ &\quad + \mu \text{diag}\{\mathbf{Q}_1(\infty) - \mathbf{Q}_4(\infty) - \mathbf{Q}_5(\infty)\}] \end{aligned} \quad (44)$$

Similar to the mean convergence analysis of ACLMS in Section III-A, in order to evaluate the terms in (43) and (44), which involves the overall noise $u(\infty)$ in (15), we need to consider the levels of the transmit power.

1) *Low transmit power:* In this case, the power of the thermal noise $v(\infty)$ in $u(\infty)$ is much higher than those of the nonlinear distortion component $\mathbf{x}_{\text{IMD}}(\infty)$ and the quantization noise $q(\infty)$, so that $E[|u(\infty)|^2] \simeq \sigma_v^2$. Since in this case $u(n) \simeq v(n)$, upon taking (30) into (39), we obtain $\mathbf{Q}_1(\infty) = \sigma_v^2 \sigma_x^2 \mathbf{I}_{2M}$, and $\mathbf{Q}_3(\infty) = \mathbf{Q}_4(\infty) = \mathbf{Q}_5(\infty) = \mathbf{0}$, and hence, $\boldsymbol{\kappa}^a(\infty)$ in (44) can be simplified as

$$\boldsymbol{\kappa}^a(\infty) = \frac{\mu\sigma_v^2}{2(1 - \mu(M+1)\sigma_x^2)} \mathbf{1}_{2M} \quad (45)$$

Upon substituting into (43), we obtain

$$J_{\text{low}}^a(\infty) = \sigma_v^2 \frac{1 - \mu\sigma_x^2}{1 - \mu(M+1)\sigma_x^2} \quad (46)$$

The achievable SNIR is defined as the relative power between the received signal of interest and the residual SI. From (7), (18), and (46), the achievable SNIR of ACLMS at the steady state can be evaluated as

$$\text{SNIR}_{\text{low}} = \frac{p_{\text{XSOI}}}{J_{\text{low}}^a(\infty)} = \frac{1 - \mu(M+1)\sigma_x^2}{1 - \mu\sigma_x^2} \text{SNR}_{\text{req}} \quad (47)$$

2) *High transmit power:* In this case, with typical parameters of FD DCTs given in Table II, the power of the SI component σ_x^2 is guaranteed to be less than unity. Therefore, in (44), the Frobenius norm of $\mu \text{diag}\{\mathbf{Q}_1(\infty) - \mathbf{Q}_4(\infty) - \mathbf{Q}_5(\infty)\}$ is much smaller than that of $\text{diag}\{\Re[\mathbf{Q}_3(\infty)]\}$, as the terms $\mathbf{Q}_1(\infty)$, $\mathbf{Q}_4(\infty)$ and $\mathbf{Q}_5(\infty)$ contain a larger amount of higher-order SI components. This situation is more pronounced when a small step-size μ is chosen, and based on the analysis in Appendix A, we have

$$\begin{aligned} &\mu \text{diag}\{\mathbf{Q}_1(\infty) - \mathbf{Q}_4(\infty) - \mathbf{Q}_5(\infty)\} + \text{diag}\{\Re[\mathbf{Q}_3(\infty)]\} \\ &= \mu(E[|v(\infty)|^2] + E[|q(\infty)|^2]) \text{diag}\{\mathbf{R}^{a*}\} + \text{diag}\{\Re[\mathbf{Q}_3(\infty)]\} \\ &\simeq \mu(\sigma_v^2 + \sigma_q^2) \sigma_v^2 \mathbf{1}_{2M} + 8k_{\text{TIQ}}^3 \sigma_x^4 \mathbf{P}_{\text{IMD}}^0 \end{aligned} \quad (48)$$

in which $\mathbf{P}_{\text{IMD}}^0$ is defined in (86). Upon replacing (48) into (44), we have

$$\boldsymbol{\kappa}^a(\infty) = \frac{\mu(\sigma_v^2 + \sigma_q^2) \mathbf{1}_{2M} + 8k_{\text{TIQ}}^3 \sigma_x^4 \mathbf{P}_{\text{IMD}}^0}{2(1 - \mu\sigma_x^2 - \mu M \sigma_x^2)} \quad (49)$$

According to (85) in Appendix A, we have

$$2\text{Tr}\{\Re[\mathbf{Q}_3(\infty)]\} = 8k_{\text{TIQ}}^3 \sigma_x^6 [\|\mathbf{h}_{\text{IMD}}^0\|_2^2 + \|\mathbf{g}_{\text{IMD}}^0\|_2^2] \quad (50)$$

and from (15),

$$E[|u(\infty)|^2] = \sigma_v^2 + \sigma_q^2 + 6k_{\text{TIQ}}^3 \sigma_x^6 [\|\mathbf{h}_{\text{IMD}}^0\|_2^2 + \|\mathbf{g}_{\text{IMD}}^0\|_2^2] \quad (51)$$

Therefore, taking (49)-(51) into (33), we arrive at

$$\begin{aligned} J_{\text{high}}^a(\infty) &= \sigma_v^2 + \sigma_q^2 - 2k_{\text{TIQ}}^3 \sigma_x^6 [\|\mathbf{h}_{\text{IMD}}^0\|_2^2 + \|\mathbf{g}_{\text{IMD}}^0\|_2^2] \\ &\quad + \frac{\mu M (\sigma_v^2 + \sigma_q^2) \sigma_x^2 + 4k_{\text{TIQ}}^3 \sigma_x^6 [\|\mathbf{h}_{\text{IMD}}^0\|_2^2 + \|\mathbf{g}_{\text{IMD}}^0\|_2^2]}{1 - \mu\sigma_x^2 - \mu M \sigma_x^2} \end{aligned} \quad (52)$$

and the achievable SNIR of ACLMS based SI canceller in the case of high transmit power is provided in (53) at the top of next page.

Remark 3: From (47) and (53), we observe that, for both low and high transmit powers, the achievable SNIRs of ACLMS at the steady state are monotonically decreasing functions of the step-size μ , the end-to-end channel IR length M , and the transmit power σ_x^2 . Particularly, in the case of high transmit powers, the achievable SNIR of ACLMS is impaired by the non-negligible IMD SI $\mathbf{x}_{\text{IMD}}(n)$ and its image $\mathbf{x}_{\text{IMD}}^*(n)$, as well as their associated end-to-end channel IRs, and its degradation becomes more severe with an increase in transmit power.

IV. PROPOSED AUGMENTED NONLINEAR CLMS (ANCLMS) BASED SI CANCELLER AND ITS PERFORMANCE ANALYSIS

From the mean and mean square analysis in Section III, it is now clear that, for high transmit powers, the third-order IMD component, produced by PA distortion, may exceed the thermal noise floor, or even become stronger than the signal of interest. This leads to bias, as well as suboptimality in SNIR performance, of the conventional ACLMS based SI canceller. To address these issues, it is desirable to design an adaptive SI canceller which jointly suppress the SI, image SI and IMD components simultaneously. Upon revisiting the vectorized signal model in (14), (15) and (20), instead of considering the IMD components $\mathbf{x}_{\text{IMD}}(n)$ and $\mathbf{x}_{\text{IMD}}^*(n)$ as a part of the aggregated noise $u(n)$, we can concatenate them with the SI component $\mathbf{x}(n)$ and its image counterpart $\mathbf{x}^*(n)$ to form a $(2M + 2N) \times 1$ augmented nonlinear SI input vector $\mathbf{x}^b(n)$, given by as

$$\mathbf{x}^b(n) = [\mathbf{x}^T(n), \mathbf{x}_{\text{IMD}}^T(n), \mathbf{x}^H(n), \mathbf{x}_{\text{IMD}}^H(n)]^T \quad (55)$$

In a similar way, we can reinterpret the widely linear baseband equivalent model from (20) into a widely-nonlinear one, given by

$$d(n) = \mathbf{x}^{bT}(n) \mathbf{w}^{bo} + v(n) + q(n) \quad (56)$$

where $\mathbf{w}^{bo} = [\mathbf{h}^{oT}, \mathbf{h}_{\text{IMD}}^{oT}, \mathbf{g}^{oT}, \mathbf{g}_{\text{IMD}}^{oT}]^T$ is the $(2M + 2N) \times 1$ sufficient-length end-to-end filter impulse response of a FD DCT. Similar to ACLMS, the proposed augmented nonlinear CLMS (ANCLMS) based SI canceller aims to estimate \mathbf{w}^{bo} by minimising a mean square error cost function $J^b(n)$, defined as

$$J^b(n) = E[|e^b(n)|^2] = E[e^b(n)e^{b*}(n)] \quad (57)$$

where the instantaneous error $e^b(n)$ is given by

$$e^b(n) = d(n) - \mathbf{x}^{bT}(n) \mathbf{w}^b(n) \quad (58)$$

and governs the update of the weight vector $\mathbf{w}^b(n)$ as

$$\mathbf{w}^b(n+1) = \mathbf{w}^b(n) + \mu e^b(n) \mathbf{x}^{b*}(n) \quad (59)$$

A. Mean Convergence Analysis

Upon introducing the $(2M + 2N) \times 1$ weight error vector

$$\tilde{\mathbf{w}}^b(n) = \mathbf{w}^b(n) - \mathbf{w}^{bo} \quad (60)$$

the output error $e^b(n)$ in (58) becomes

$$e^b(n) = v(n) + q(n) - \mathbf{x}^{bT}(n) \tilde{\mathbf{w}}^b(n) \quad (61)$$

and the recursion of $\tilde{\mathbf{w}}^b(n)$ can now be derived as

$$\begin{aligned} \tilde{\mathbf{w}}^b(n+1) &= [\mathbf{I}_{2M+2N} - \mu \mathbf{x}^{b*}(n) \mathbf{x}^{bT}(n)] \tilde{\mathbf{w}}^b(n) \\ &\quad + \mu [v(n) + q(n)] \mathbf{x}^{b*}(n) \end{aligned} \quad (62)$$

Taking the expectation operator $E[\cdot]$ on both sides of (62) and using the standard independence assumptions introduced in Section III-A, we arrive at

$$E[\tilde{\mathbf{w}}^b(n+1)] = [\mathbf{I}_{2M+2N} - \mu \mathbf{R}^b] E[\tilde{\mathbf{w}}^b(n)] \quad (63)$$

where \mathbf{I}_{2M+2N} is an identity matrix of size $(2M + 2N)$, and $\mathbf{R}^b = E[\mathbf{x}^b(n) \mathbf{x}^{bH}(n)]$ is the covariance matrix of the augmented nonlinear SI input vector $\mathbf{x}^b(n)$. Based on (63), the step-size μ which guarantees the convergence of the proposed ANCLMS in the mean sense should satisfy [39]

$$|1 - \mu \lambda_k^b| < 1, \quad k = 1, \dots, 2M + 2N \quad (64)$$

where λ_k^b are the eigenvalues of \mathbf{R}^b . Note that although \mathbf{R}^b is Hermitian, its positive-definiteness is not always guaranteed due to the non-Gaussianity of $\mathbf{x}^b(n)$. To investigate this issue, we shall further decompose \mathbf{R}^b as

$$\mathbf{R}^b = E[\mathbf{x}^b(n) \mathbf{x}^{bH}(n)] = \begin{bmatrix} \mathbf{R}_0^b & \mathbf{0} \\ \mathbf{0} & \mathbf{R}_0^b \end{bmatrix} \quad (65)$$

where

$$\mathbf{R}_0^b = E[\mathbf{x}^c(n) \mathbf{x}^{cH}(n)] = \begin{bmatrix} E[|x|^2] \mathbf{I}_M & \boldsymbol{\Omega}^T \\ \boldsymbol{\Omega} & k_{\text{TIQ}}^3 E[|x|^6] \mathbf{I}_N \end{bmatrix}$$

$$\boldsymbol{\Omega} = [\mathbf{R}^d \quad \mathbf{0}_{N \times (M-N)}]$$

$$\mathbf{R}^d = E[\mathbf{x}^d(n) \mathbf{x}_{\text{IMD}}^H(n)] = k_{\text{TIQ}}^{3/2} E[|x|^4] \mathbf{I}_N$$

and $\mathbf{x}^c(n) = [\mathbf{x}^T(n), \mathbf{x}_{\text{IMD}}^T(n)]^T$ and $\mathbf{x}^d(n) = [x(n), x(n-1), \dots, x(n-N+1)]^T$. Now, by solving $\det[\mathbf{R}^b - \lambda_k^b \mathbf{I}_{2M+2N}] = 0$ and after a few manipulations, we arrive at

$$\begin{aligned} \lambda_1^b &= E[|x|^2] = \sigma_x^2 \\ \lambda_{2,3}^b &= \frac{1}{2} \left\{ E[|x|^2] + k_{\text{TIQ}}^3 E[|x|^6] \right. \\ &\quad \left. \pm \sqrt{(E[|x|^2] + k_{\text{TIQ}}^3 E[|x|^6])^2 - k_{\text{TIQ}}^3 E^2[|x|^4]} \right\} \\ &= \frac{\sigma_x^2 + 6k_{\text{TIQ}}^3 \sigma_x^6 \pm \sqrt{(\sigma_x^2 + 6k_{\text{TIQ}}^3 \sigma_x^6)^2 - 8k_{\text{TIQ}}^3 \sigma_x^8}}{2} \end{aligned} \quad (66)$$

where the algebraic multiplicities of λ_1^b , λ_2^b and λ_3^b are respectively $2M - 2N$, $2N$ and $2N$.

Remark 4: The covariance matrix \mathbf{R}^b is positive-definite since all the eigenvalues are positive. It is also worth noting that, although $x(n)$ is considered to be i.i.d. Gaussian, the positive definiteness of \mathbf{R}^b is still valid as long as $x(n)$ comes from any i.i.d. second-order circular constellation, e.g., QPSK or M-QAM.

Note that in (66), the largest eigenvalue of \mathbf{R}^b is λ_2^b , and therefore, the mean convergence bound on the step-size μ is given by

$$\begin{aligned} 0 < \mu &< \frac{2}{\lambda_{\max}[\mathbf{R}^b]} \\ &= \frac{4}{\sigma_x^2 + 6k_{\text{TIQ}}^3 \sigma_x^6 + \sqrt{(\sigma_x^2 + 6k_{\text{TIQ}}^3 \sigma_x^6)^2 - 8k_{\text{TIQ}}^3 \sigma_x^8}} \end{aligned} \quad (67)$$

$$\text{SNIR}_{\text{high}} = \frac{p_{\text{SOI}}}{J_{\text{high}}^a(\infty)} = \frac{1 - \mu(M+1)\sigma_x^2}{\left(\frac{1}{\text{SNR}_{\text{req}}} + \frac{\sigma_q^2}{k_{\text{BB}}k_{\text{LNA}}k_{\text{TIQ}}p_{\text{sen}}}\right) + \frac{2[1 + \mu(M+1)\sigma_x^2]k_{\text{TIQ}}^2\sigma_x^6(\|\mathbf{h}_{\text{IMD}}^o\|_2^2 + \|\mathbf{g}_{\text{IMD}}^o\|_2^2)}{k_{\text{BB}}k_{\text{LNA}}p_{\text{sen}}}} \quad (53)$$

which enables the proposed ANCLMS based SI canceller to asymptotically achieve unbiased estimation of the optimal weight vector \mathbf{w}^{bo} , indicated by $E[\tilde{\mathbf{w}}^b(\infty)] = \mathbf{0}$ and based on (63), independent on whether the transmit power of an FD DCT is low or high.

B. Mean Square Convergence Analysis

Upon taking (61) into (57), and again employing the standard independence assumptions, the MSE of the proposed ANCLMS based SI canceller can be further evaluated as

$$J^b(n) = \text{Tr}[\mathbf{R}^b \mathbf{K}^b(n)] + \sigma_v^2 + \sigma_q^2 \quad (68)$$

where $\mathbf{K}^b(n) = E[\tilde{\mathbf{w}}^b(n)\tilde{\mathbf{w}}^{bH}(n)]$ is the covariance matrix of the weight error vector $\tilde{\mathbf{w}}^b(n)$. To analyze its evolution, we first multiply both sides of (62) by $\tilde{\mathbf{w}}^{bH}(n)$, and apply the statistical expectation operator $E[\cdot]$ on them, to give

$$\begin{aligned} \mathbf{K}^b(n+1) &= \mathbf{K}^b(n) + \mu^2(\sigma_v^2 + \sigma_q^2)\mathbf{R}^b \\ &\quad - \mu E[\mathbf{x}^{b*}(n)\mathbf{x}^{bT}(n)\tilde{\mathbf{w}}^b(n)\tilde{\mathbf{w}}^{bH}(n)] \\ &\quad - \mu E[\tilde{\mathbf{w}}^b(n)\tilde{\mathbf{w}}^{bH}(n)\mathbf{x}^{b*}(n)\mathbf{x}^{bT}(n)] \\ &\quad + \mu^2 E[\mathbf{x}^{b*}(n)\mathbf{x}^{bT}(n)\tilde{\mathbf{w}}^b(n)\tilde{\mathbf{w}}^{bH}(n)\mathbf{x}^{b*}(n)\mathbf{x}^{bT}(n)] \end{aligned} \quad (69)$$

Since the augmented nonlinear SI vector $\mathbf{x}^b(n)$ in (55) is non-Gaussian, the Gaussian fourth order moment factorising theorem used in Section III is no longer applicable to evaluate the last term on the RHS of (69), and we therefore resort to matrix vectorization instead of matrix diagonalization to evaluate the mean square convergence behavior of the proposed ANCLMS [48], [49]. By using the following matrix vectorization lemma for arbitrary matrices $\{\mathbf{A}, \mathbf{B}, \mathbf{C}\}$

$$\text{vec}\{\mathbf{ABC}\} = (\mathbf{C}^T \otimes \mathbf{A})\text{vec}\{\mathbf{B}\}$$

it is straightforward to verify that the recursion for $\mathbf{K}^b(n)$ in (69) can be transformed into a linear vector relation as

$$\begin{aligned} \text{vec}\{\mathbf{K}^b(n+1)\} &= \underbrace{(\mathbf{I}_{2M+2N} - \mu\mathbf{S} + \mu^2\mathbf{T})}_{\mathbf{F}^b} \text{vec}\{\mathbf{K}^b(n)\} \\ &\quad + \mu^2(\sigma_v^2 + \sigma_q^2)\text{vec}\{\mathbf{R}^b\} \end{aligned} \quad (70)$$

where

$$\mathbf{S} = \mathbf{I}_{2M+2N} \otimes \mathbf{R}^b + \mathbf{R}^b \otimes \mathbf{I}_{2M+2N} \quad (71)$$

$$\mathbf{T} = E[(\mathbf{x}^b(n)\mathbf{x}^{bH}(n)) \otimes (\mathbf{x}^{b*}(n)\mathbf{x}^{bT}(n))] \quad (72)$$

The condition on the step-size μ to guarantee the convergence of $\mathbf{K}^b(n)$ now relies on $|\lambda[\mathbf{F}^b]| < 1$. It has been proved in [49] that for positive definite \mathbf{R}^b and \mathbf{S} and nonnegative definite \mathbf{T} , the stability of the recursion in (70) is guaranteed when

$$0 < \mu < \min \left\{ \frac{1}{\lambda_{\max}(\mathbf{S}^{-1}\mathbf{T})}, \frac{1}{\max\{\lambda(\Gamma) \in \mathbb{R}^+\}} \right\} \quad (73)$$

where

$$\Gamma = \begin{bmatrix} \frac{\mathbf{S}}{2} & -\frac{\mathbf{T}}{2} \\ \mathbf{I}_{(2M+2N)^2} & \mathbf{0} \end{bmatrix} \quad (74)$$

C. Steady State Analysis

Suppose the step-size μ is chosen to ensure the mean square stability of the proposed ANCLMS, from (68), the steady-state MSE $J^b(\infty)$ can be expressed as

$$J^b(\infty) = \text{Tr}[\mathbf{R}^b \mathbf{K}^b(\infty)] + \sigma_v^2 + \sigma_q^2 \quad (75)$$

in which $\mathbf{K}^b(\infty)$ can be evaluated from (70) as

$$\begin{aligned} \mathbf{K}^b(\infty) &= \text{vec}^{-1}\{\mu^2(\sigma_v^2 + \sigma_q^2)(\mathbf{I}_{2M+2N} - \mathbf{F}^b)^{-1}\text{vec}\{\mathbf{R}^b\}\} \\ &= \text{vec}^{-1}\{\mu^2(\sigma_v^2 + \sigma_q^2)(\mu\mathbf{S} - \mu^2\mathbf{T})^{-1}\text{vec}\{\mathbf{R}^b\}\} \end{aligned} \quad (76)$$

By substituting (76) into (75), we have

$$J^b(\infty) = (\sigma_v^2 + \sigma_q^2)(1 + \mu^2 \text{Tr}[\mathbf{R}^b \text{vec}^{-1}\{(\mu\mathbf{S} - \mu^2\mathbf{T})^{-1}\text{vec}\{\mathbf{R}^b\}\}])$$

Due to the existence of the fourth-order moment matrix \mathbf{T} , a detailed evaluation of the steady state MSE $J^b(\infty)$ is much more difficult than that of the standard ACLMS. However, as shown in (70), matrix \mathbf{T} is multiplied by μ^2 within the matrix \mathbf{F}^b , then for a sufficient small step-size μ , we can neglect the term $\mu^2\mathbf{T}$ in \mathbf{F}^b . In this way, by applying the standard eigenvalue decomposition (EVD) on \mathbf{R}^b to give $\mathbf{R}^b = \mathbf{U}\mathbf{\Lambda}^b\mathbf{U}^H$, in which \mathbf{U} is a unitary matrix and $\mathbf{\Lambda}^b = \text{diag}\{\lambda_1^b, \lambda_2^b, \dots, \lambda_{2M+2N}^b\}$ is a diagonal matrix comprising of the eigenvalues of \mathbf{R}^b , from (69), we have

$$\tilde{\mathbf{K}}^b(n+1) = \tilde{\mathbf{K}}^b(n) + \mu^2(\sigma_v^2 + \sigma_q^2)\mathbf{\Lambda}^b - \mu\mathbf{\Lambda}^b\tilde{\mathbf{K}}^b(n) - \mu\tilde{\mathbf{K}}^b(n)\mathbf{\Lambda}^b \quad (77)$$

where $\tilde{\mathbf{K}}^b(n) = \mathbf{U}^H \mathbf{K}^b(n) \mathbf{U}$, and its steady-state value $\tilde{\mathbf{K}}^b(\infty)$ can be obtained as

$$\tilde{\mathbf{K}}^b(\infty) = \frac{\mu(\sigma_v^2 + \sigma_q^2)}{2} \mathbf{I}_{2M+2N} \quad (78)$$

Upon substituting into (75), we obtain an approximated steady-state MSE, denoted by $J_{\text{ap}}^b(\infty)$, in the form

$$\begin{aligned} J_{\text{ap}}^b(\infty) &= \text{Tr}[\mathbf{U}\mathbf{\Lambda}^b\tilde{\mathbf{K}}^b(\infty)\mathbf{U}^H] + \sigma_v^2 + \sigma_q^2 \\ &= (\sigma_v^2 + \sigma_q^2)[\mu(M\sigma_x^2 + 6Nk_{\text{TIQ}}^3\sigma_x^6) + 1] \end{aligned} \quad (79)$$

Now from (7), (18) and (79), the achievable SNIR of the proposed ANCLMS can be evaluated as in (80) at the top of next page.

Remark 5: The achievable SNIR of the proposed ANCLMS based SI canceller in (80) is a monotonically decreasing function of the step-size μ , the length of SI channel IR M and that of IMD SI channel IR N , the transmitter mixer gain k_{TIQ} , and the SI power σ_x^2 . Moreover, in the situations of high transmit powers, owing to the model fitting advantage, the optimality of the proposed ANCLMS for SI cancellation can be also observed, since its achievable SNIR is no longer impaired by the IMD channel IRs, that is, $\|\mathbf{h}_{\text{IMD}}^o\|_2^2$ and $\|\mathbf{g}_{\text{IMD}}^o\|_2^2$, which, however, remain the by-products of the undermodeling problem encountered by the conventional ACLMS based SI canceller for FD DCTs in the joint presence of PA nonlinearity and frequency-dependent IQ imbalances.

$$\text{SNIR}_{\text{ANCLMS}} = \frac{p_{\text{xSOI}}}{J_{\text{ap}}^b(\infty)} = \frac{1}{\left[\frac{1}{\text{SNR}_{\text{req}}} + \frac{\sigma_q^2}{k_{\text{BB}} k_{\text{LNA}} k_{\text{TIQ}} p_{\text{sen}}} \right] [1 + \mu(M\sigma_x^2 + 6Nk_{\text{TIQ}}^3\sigma_x^6)]} \quad (80)$$

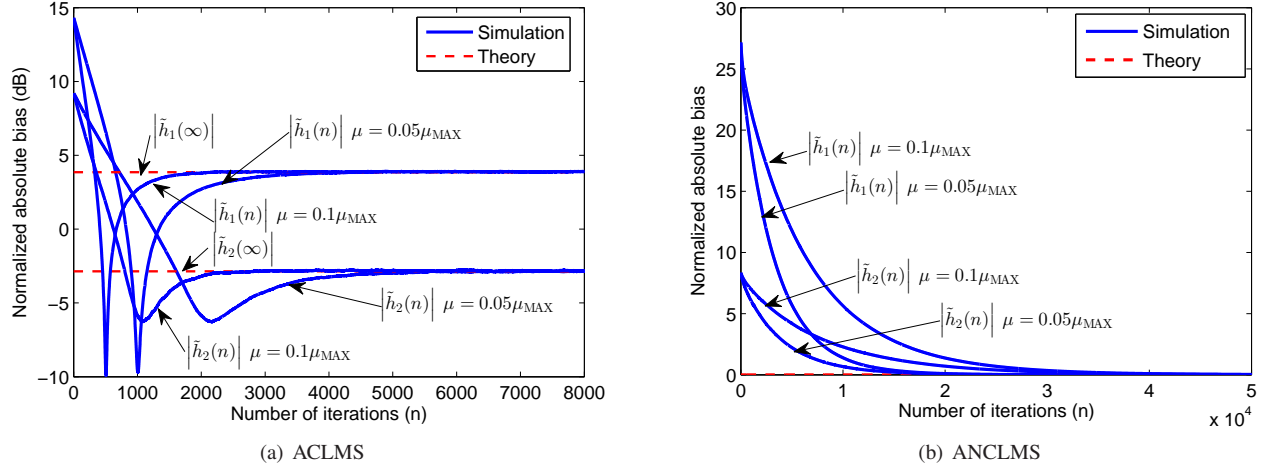


Fig. 3. Normalized absolute values of two representative error coefficients $\tilde{h}_1(n)$ and $\tilde{h}_2(n)$ for a Type 2 FD DCT by using (a) ACLMS and (b) ANCLMS, where $\mu \in \{0.05\mu_{\text{max}}, 0.1\mu_{\text{max}}\}$.

V. COMPUTER SIMULATIONS

In order to validate the performance advantages of the proposed ANCLMS based digital SI canceller over the conventional ACLMS one for full-duplex direct-conversion transceivers (FD DCTs) in the presence of PA nonlinear distortion and frequency-dependent IQ imbalances, simulations were conducted in the MATLAB programming environment. The simulated waveforms of the transmit SI $x(n)$ and the received signal of interest $x_{\text{SOI}}(n)$ were both considered to be generated from OFDM transmission systems compliant with the wireless LAN (WLAN) 802.11 standards. The numbers of subcarriers and null subcarriers of the WLAN-OFDM transmission system were respectively $K = 64$ and $K_{\text{null}} = 14$. The length of cyclic prefix was $K_{\text{cp}} = 16$, the oversampling factor was $K_{\text{os}} = 4$, and the waveform bandwidth was $B_c = 20$ MHz, to give an OFDM symbol duration $T_{\text{sym}} = (K + K_{\text{cp}})/B_c = 4 \mu\text{s}$. The 16-QAM constellation scheme was used in each subcarrier. The residual analog cancellation error was subject to a 3-tap static Rayleigh distribution, whose detailed power-delay-profile is provided in [8]. The frequency-dependent transmitter and receiver I/Q imbalance IRs were both modeled as 2-tap static FIR filters [33]. In this way, the length of the end-to-end channel IRs for the SI $\mathbf{x}(n)$ and its image component $\mathbf{x}^*(n)$, that is, \mathbf{h}^0 and \mathbf{g}^0 , was set to $M = 5$, while that for the IMD components $\mathbf{x}_{\text{IMD}}(n)$ and $\mathbf{x}_{\text{IMD}}^*(n)$, that is, $\mathbf{h}_{\text{IMD}}^0$ and $\mathbf{g}_{\text{IMD}}^0$, was set to $N = 4$. All the simulation results were obtained by averaging 200 independent trials.

As stated in **Remark 1**, for high Tx powers, ACLMS based SI canceller yields an unavoidable steady-state bias on the estimation of $2N$ out of $2M$ entries of the augmented optimal end-to-end system IRs $\mathbf{w}^{\text{ao}} = [\mathbf{h}^{\text{oT}}, \mathbf{g}^{\text{oT}}]^T$, due to

the arbitrary negligence of the IMD SI components, and this bias is quantified by (32). This analysis is supported by Fig. 3(a), in which the evolutions of two representative weight error coefficients, that is, $\tilde{h}_1(n)$ and $\tilde{h}_2(n)$, are provided. A Type 2 FD DCT with a transmit power at 25 dBm was considered, and two step-sizes $\mu = 0.05\mu_{\text{max}}$ and $\mu = 0.1\mu_{\text{max}}$ were used in ACLMS, where μ_{max} is the upper bound of the step-size μ , which guarantees both the mean and mean square stability of ACLMS, evaluated by using (42). Observe that the two weight error coefficients, $\tilde{h}_1(n)$ and $\tilde{h}_2(n)$ converged to their theoretical steady-state values, rather than 0. However, as discussed in Section IV, due to the appropriate model fitting, the proposed ANCLMS based SI canceller is able to remove this bias, as illustrated in Fig. 3(b). Note that the maximum step-size μ_{max} for ANCLMS was considered as the lower value of the upper bounds given in (67) and (73), so as to guarantee its convergence in both mean and mean square senses.

We next validated the proposed mean square analysis of both ACLMS and ANCLMS based SI cancellers. Fig. 4(a) illustrates the theoretical and simulated achievable SNIRs in the steady-state stage, with $\mu = 0.05\mu_{\text{max}}$ and $\mu = 0.1\mu_{\text{max}}$ and against different levels of transmit powers for a Type 2) FD DCT. Observe that the empirical results were closely matched with the analytical ones, evaluated by using (53) and (80) respectively for ACLMS and ANCLMS. These also conform with the analysis in **Remark 3** and **Remark 5** which states that a smaller step-size μ enables a better steady-state SNIR performance for both SI cancellers, but at the cost of slower convergence. Fig. 4(a) also justifies the motivations to propose the ANCLMS based SI canceller in the sense that its SNIR performance is much better than that of ACLMS in the high transmit power range where the IMD SI component

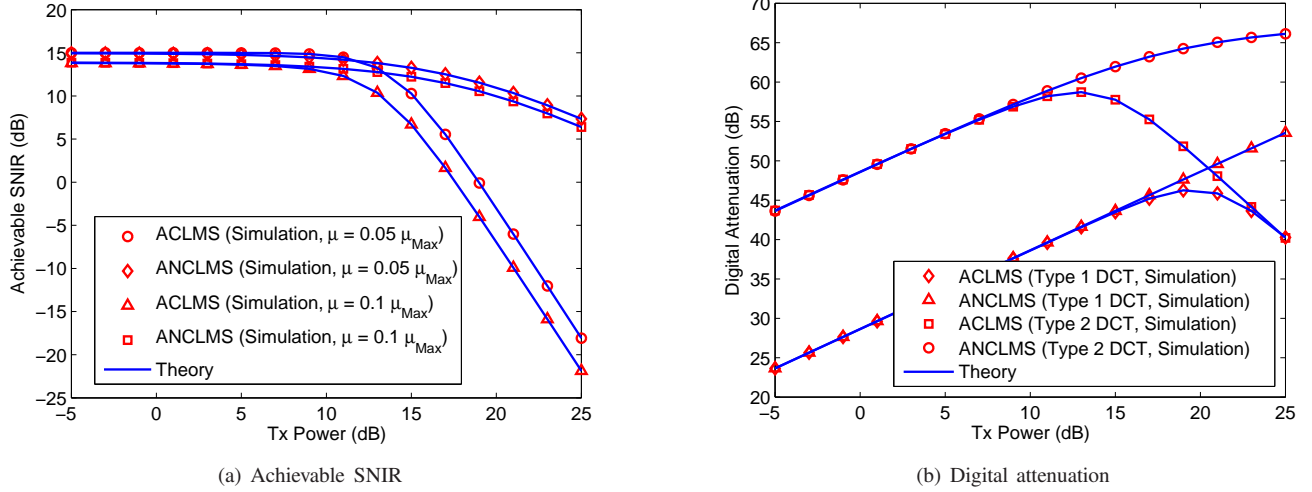


Fig. 4. Comparison of the theoretical and simulated steady-state mean square performances of both the conventional ACLMS and the proposed ANCLMS, measured in terms of (a) Achievable SNIR, and (b) Digital attenuation.

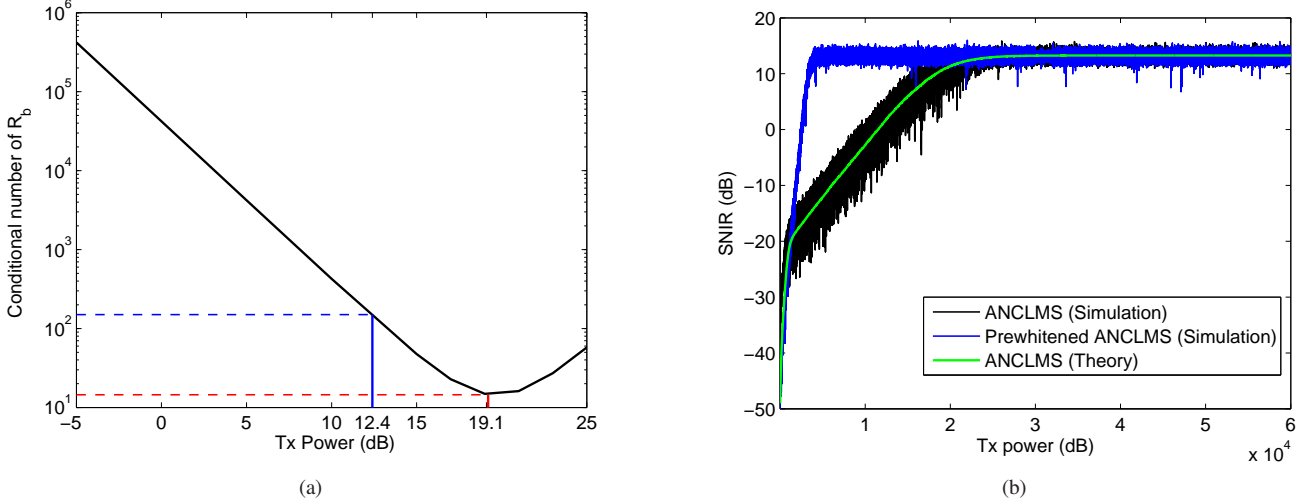


Fig. 5. Convergence speed analysis and the benefits of the proposed ANCLMS. (a) The variations of the condition number of \mathbf{R}^b against the levels of transmit power. The solid lines, labeled in red and blue respectively, indicate the positions where the power of IMD SI component $\mathbf{x}_{\text{IMD}}(n)$ became stronger than that of thermal noise $v(n)$ in both Type 1 and Type 2 FD DCTs. (b) Performance comparison between the theoretical and simulated SNIR of ANCLMS and the simulated SNIR of its prewhitened counterpart for Type 2 FD DCTs, with $\mu = 0.05\mu_{\max}$.

$\mathbf{x}_{\text{IMD}}(n)$ and its image counterpart become dominant, since both components have been generically considered as a part of the augmented nonlinear input vector within the proposed ANCLMS. As expected, when the transmit power was low enough, both SI cancellers provided a nearly identical SNIR performance, since the higher order components became negligible. This also resulted in the theoretical SNIR performance of ACLMS in (53), derived for a high transmit power, asymptotically converge to that in (47). The above discussion is also applicable for Fig. 4(b), where we compared the digital attenuation capability of the two considered SI cancellers after convergence with a step-size $\mu = 0.05\mu_{\max}$, for both Type 1 and Type 2 FD DCTs and against different levels of transmit powers. The digital attenuation performance is a measure of the amount of SI before and after applying an SI canceller,

defined as the power ratio between the desired signal $d(n)$ and the corresponding estimation error of an SI canceller [27]. Observe the excellent agreement between the simulated results and their theoretical evaluations, as well as the performance advantages of the proposed ANCLMS over the conventional ACLMS in the high transmit power range.

A. Further Convergence Speed Improvement of the Proposed ANCLMS based SI Cancellor

With an increase in the transmit power of a FD DCT, the contribution of the higher-order IMD component $\mathbf{x}_{\text{IMD}}(n)$ to the covariance matrix \mathbf{R}^b of the augmented nonlinear SI vector $\mathbf{x}^b(n)$ become stronger for a FD DCT in the joint presence of nonlinear PA distortion and IQ imbalances. This makes \mathbf{R}^b prone to a high eigenvalue spread, and consequently

results in a slow convergence of the proposed ANCLMS [19]. This phenomenon becomes clearer from Fig. 5(a), where the variations on the condition number of \mathbf{R}^b , i.e., the ratio between its maximum and minimum eigenvalues, that is, λ_2^b/λ_3^b , against different levels of transmit powers were investigated. It can be observed that the transmit power ranges between 19.1 dB and 25 dB and between 12.4 dB to 25 dB were respectively the regions where the convergence of the proposed ANCLMS began to decelerate in Type 1 and Type 2 FD DCTs. More specifically, in a Type 1 DCT, the slow convergence took place only when the transmit power approached its maximum, however, this problem was more severe in Type 2 DCT, as the condition number of \mathbf{R}^b was as large as 200 when the IMD SI component $\mathbf{x}_{\text{IMD}}(n)$ became dominant. There are many approaches that can be used to alleviate the slow convergence problem, and since the closed-form expression of \mathbf{R}^b is available, we here resort to the standard pre-whitening solution. Note that the covariance matrix \mathbf{R}^b can be decomposed as $\mathbf{R}^b = \mathbf{U}\mathbf{\Lambda}^b\mathbf{U}^H$, and hence, its corresponding whitening transformation matrix can be obtained as $\mathbf{\Phi} = [\mathbf{\Lambda}^b]^{-\frac{1}{2}}\mathbf{U}^H$, which produces a whitened input vector as $\tilde{\mathbf{x}}^b(n) = \mathbf{\Phi}\mathbf{x}^b(n)$. In this way, the speed of gradient decent of ANCLMS is fixed, facilitating its practical applications. This is supported by Fig. 5(b), which shows both the theoretical and simulated convergence behaviors, measured in terms of SNIR, of the proposed ANCLMS based SI canceller and its data-whitening assisted version for a Type 2 FD DCT with a transmit power at 15 dBm and a step-size at $\mu = 0.05\mu_{\text{max}}$. The theoretical SNIR of ANCLMS was calculated as $p_{\text{XSOI}}/J^b(n)$, where $J^b(n)$ was evaluated by using (68), whose convergence was governed by that of the augmented weight error covariance matrix $\mathbf{K}^b(n)$ in (69). We observe that the proposed theoretical evaluation accurately described the empirical SNIR evolution of ANCLMS in both transient and steady-state stages. We also observe that the prewhitening scheme equipped ANCLMS with a much faster convergence, since it stabilized the eigenvalue spread of the covariance matrix \mathbf{R}^b , e.g., it required about 3000 iterations to achieve its steady state, while in contrast, this process cost about 25000 iterations for the original ANCLMS.

VI. CONCLUSION

The impacts of typical front-ends nonidealities on a future 5G systems, such as nonlinear PA distortion, IQ imbalances, thermal noise and quantization noise, has been rigorously analyzed over both the mean and mean square performances of the conventional ACLMS based digital SI canceller for fully-duplex direct-conversion transceivers (FD DCTs). We have established that a high transmit power leads the third-order intermodulation components and their image counterparts, which are non-ignorable interferences within FD DCTs. This consequently results in both the estimation bias and performance suboptimality exhibited by ACLMS after convergence. To rectify these drawbacks, an augmented nonlinear CLMS (ANCLMS) based SI canceller has been proposed, which naturally accounts for those higher-order components by virtue of a widely-nonlinear model fit. Its performance

advantages over ACLMS has been justified both theoretically and through numerical validation. To further increase its convergence speed, the standard data pre-whitening scheme has also been employed in this context. Illustrative simulations on two representative types of FD DCTs for OFDM-based WLAN standard compliant waveforms support the analysis.

APPENDIX A

EVALUATION OF THE TERM $\text{diag}\{\mathbf{Q}_3(\infty)\}$ IN THE CASE OF HIGH TRANSMIT POWER

Based on (15) and (35), the diagonal elements of $\mathbf{Q}_3(n)$ can be derived as

$$\begin{aligned} & \text{diag}\{E[\mathbf{Q}_3(n)]\} \\ &= \text{diag}\{E[\mathbf{x}_{\text{IMD}}^T(n)\mathbf{h}_{\text{IMD}}^o(n)\mathbf{x}^{a*}(n)]E[\tilde{\mathbf{w}}^{aH}(n)]\} \\ &+ \text{diag}\{E[\mathbf{x}_{\text{IMD}}^H(n)\mathbf{g}_{\text{IMD}}^o(n)\mathbf{x}^{a*}(n)]E[\tilde{\mathbf{w}}^{aH}(n)]\} \\ &+ \text{diag}\{E[v(n)\mathbf{x}^{a*}(n)]E[\tilde{\mathbf{w}}^{aH}(n)]\} \end{aligned} \quad (82)$$

while the standard independence assumptions yield

$$\text{diag}\{E[v(n)\mathbf{x}^{a*}(n)]E[\tilde{\mathbf{w}}^{aH}(n)]\} = \mathbf{0} \quad (83)$$

Now, based on (31) and (83), we have

$$\begin{aligned} & \text{diag}\{E[\mathbf{Q}_3(n)]\} = [h_{\text{IMD},1}k_{\text{TIQ}}^{3/2}E[|x(n)|^4]E[\tilde{w}_1^*(n)], \\ & h_{\text{IMD},2}k_{\text{TIQ}}^{3/2}E[|x(n-1)|^4]E[\tilde{w}_2^*(n)], \dots, \\ & h_{\text{IMD},N}k_{\text{TIQ}}^{3/2}E[|x(n-N+1)|^4]E[\tilde{w}_N^*(n)], \mathbf{0}_{M-N}^T, \\ & g_{\text{IMD},1}k_{\text{TIQ}}^{3/2}E[|x(n)|^4]E[\tilde{w}_1^*(n)], \dots, \\ & g_{\text{IMD},N}k_{\text{TIQ}}^{3/2}E[|x(n)|^4]E[\tilde{w}_N^*(n)], \mathbf{0}_{M-N}^T] \end{aligned} \quad (84)$$

Note that $E[|x(n)|^4] = 2\sigma_x^4$, and hence, the steady-state evaluation of $\text{diag}\{E[\mathbf{Q}_3(n)]\}$, that is, $\text{diag}\{E[\mathbf{Q}_3(\infty)]\}$, is now subject to $E[\tilde{\mathbf{w}}^a(\infty)]$, and based on (32), this gives

$$\text{diag}\{\mathbf{Q}_3(\infty)\} = 4k_{\text{TIQ}}^3\sigma_x^6\mathbf{p}_{\text{IMD}}^o \quad (85)$$

where $\mathbf{p}_{\text{IMD}}^o$ is defined as

$$\begin{aligned} \mathbf{p}_{\text{IMD}}^o &= [|h_{\text{IMD},1}|^2, |h_{\text{IMD},2}|^2, \dots, |h_{\text{IMD},N}|^2, \mathbf{0}_{M-N}^T, \\ & |g_{\text{IMD},1}|^2, |g_{\text{IMD},2}|^2, \dots, |g_{\text{IMD},N}|^2, \mathbf{0}_{M-N}^T]^T \end{aligned} \quad (86)$$

Also note that $\Re\{\mathbf{Q}_3(\infty)\} = \mathbf{Q}_3(\infty)$, since it is real-valued.

REFERENCES

- [1] S. Hong, J. Brand, J. Choi, M. Jain, J. Mehlman, S. Katti, and P. Levis, "Applications of self-interference cancellation in 5G and beyond," *IEEE Commun. Mag.*, vol. 52, no. 2, pp. 114–121, Feb. 2014.
- [2] A. C. Cirik, Y. Rong, and Y. Hua, "Achievable rates of full-duplex MIMO radios in fast fading channels with imperfect channel estimation," *IEEE Trans. Signal Process.*, vol. 62, no. 15, pp. 3874–3886, Jun. 2014.
- [3] D. Kim, H. Lee, and D. Hong, "A survey of in-band full-duplex transmission: from the perspective of PHY and MAC layers," *IEEE Commun. Surv. Tutorials*, vol. 17, no. 4, pp. 2017–2046, Fourth quarter 2015.
- [4] A. Sabharwal, P. Schniter, D. Guo, D. W. Bliss, S. Rangarajan, and R. Wichman, "In-band full-duplex wireless: Challenges and opportunities," *IEEE J. Sel. Areas Commun.*, vol. 32, no. 9, pp. 1637–1652, Sep. 2014.
- [5] K. E. Kolodziej, J. G. McMichael, and B. T. Perry, "Multitap RF canceller for in-band full-duplex wireless communications," *IEEE Trans. Wirel. Commun.*, vol. 15, no. 6, pp. 4321–4334, Jun. 2016.
- [6] J. Choi, M. Jain, and K. Srinivasan, "Achieving single channel, full duplex wireless communication," in *Proc. ACM Mobicom*, Sep. 2010, pp. 1–12.
- [7] M. Jain, J. I. Choi, T. Kim, D. Bharadia, S. Seth, K. Srinivasan, P. Levis, S. Katti, and P. Sinha, "Practical, real-time, full duplex wireless," in *Proc. ACM MobiCom*, Sep. 2011, pp. 301–312.

- [8] M. Duarte, C. Dick, and A. Sabharwal, "Experiment-driven characterization of full-duplex wireless systems," *IEEE Trans. Wirel. Commun.*, vol. 11, no. 12, pp. 4296–4307, Dec. 2012.
- [9] D. Bharadia, E. McMillin, and S. Katti, "Full duplex radios," in *Proc. ACM SIGCOMM*, vol. 43, no. 4, Aug. 2013, p. 375.
- [10] D. Bharadia, S. Katti, and I. Nsdi, "Full duplex MIMO radios," in *Proc. 11th USENIX Symp. NSDI*, Apr. 2014, pp. 359–372.
- [11] E. Everett, A. Sahai, and A. Sabharwal, "Passive self-interference suppression for full-duplex infrastructure nodes," *IEEE Trans. Wirel. Commun.*, vol. 13, no. 2, pp. 680–694, Feb. 2014.
- [12] E. Everett, M. Duarte, C. Dick, and A. Sabharwal, "Empowering full-duplex wireless communication by exploiting directional diversity," in *Proc. 45th Asilomar Conf. on Signals, Syst. Comput. (ASILOMAR)*, Nov. 2011, pp. 2002–2006.
- [13] S. Goyal, P. Liu, S. S. Panwar, R. A. DiFazio, R. Yang, and E. Bala, "Full duplex cellular systems: Will doubling interference prevent doubling capacity?" *IEEE Commun. Mag.*, vol. 53, no. 5, pp. 121–127, May 2015.
- [14] D. Korpi, J. Tamminen, M. Turunen, T. Huusari, Y. S. Choi, L. Anttila, S. Talwar, and M. Valkama, "Full-duplex mobile device: Pushing the limits," *IEEE Commun. Mag.*, vol. 54, no. 9, pp. 80–87, Sep. 2016.
- [15] A. Sahai, S. Diggavi, and A. Sabharwal, "On degrees-of-freedom of full-duplex uplink/downlink channel," in *Proc. IEEE ITW*, Sep. 2013, pp. 1–5.
- [16] T. Snow, C. Fulton, and W. J. Chappell, "Transmit-receive duplexing using digital beamforming system to cancel self-interference," *IEEE Trans. Microw. Theory Tech.*, vol. 59, no. 12 PART 2, pp. 3494–3503, Dec. 2011.
- [17] T. Riihonen, S. Werner, and R. Wichman, "Mitigation of loopback self-interference in full-duplex MIMO relays," *IEEE Trans. Signal Process.*, vol. 59, no. 12, pp. 5983–5993, Dec. 2011.
- [18] Y. S. Choi and H. Shirani-Mehr, "Simultaneous transmission and reception: Algorithm, design and system level performance," *IEEE Trans. Wirel. Commun.*, vol. 12, no. 12, pp. 5992–6010, Dec. 2013.
- [19] L. Anttila, D. Korpi, V. Syrjälä, and M. Valkama, "Cancellation of power amplifier induced nonlinear self-interference in full-duplex transceivers," *Proc. 47th Asilomar Conf. on Signals, Syst. Comput. (ASILOMAR)*, pp. 1193–1198, 2013.
- [20] D. Korpi, T. Riihonen, V. Syrjälä, L. Anttila, M. Valkama, and R. Wichman, "Full-duplex transceiver system calculations: Analysis of ADC and linearity challenges," *IEEE Trans. Wirel. Commun.*, vol. 13, no. 7, pp. 3821–3836, Jul. 2014.
- [21] V. Syrjälä, M. Valkama, L. Anttila, T. Riihonen, and D. Korpi, "Analysis of oscillator phase-noise effects on self-interference cancellation in full-duplex OFDM radio transceivers," *IEEE Trans. Wirel. Commun.*, vol. 13, no. 6, pp. 2977–2990, Jun. 2014.
- [22] X. Quan, Y. Liu, S. Shao, C. Huang, and Y. Tang, "Impacts of phase noise on digital self-interference cancellation in full-duplex communications," *IEEE Trans. Signal Process.*, vol. 65, no. 7, pp. 1881–1893, Apr. 2017.
- [23] A. Tarighat, R. Bagheri, and A. H. Sayed, "Compensation schemes and performance analysis of IQ imbalances in OFDM receivers," *IEEE Trans. Signal Process.*, vol. 53, no. 8, pp. 3257–3268, Aug. 2005.
- [24] L. Anttila, M. Valkama, and M. Renfors, "Frequency-selective I/Q mismatch calibration of wideband direct-conversion transmitters," *IEEE Trans. Circuits Syst. II*, vol. 55, no. 4, pp. 359–363, Apr. 2008.
- [25] Z. Li, Y. Xia, W. Pei, K. Wang, Y. Huang, and D. P. Mandic, "Noncircular measurement and mitigation of I/Q imbalance for OFDM-based WLAN transmitters," *IEEE Trans. Instrum. Meas.*, vol. 66, no. 3, pp. 383–393, Mar. 2017.
- [26] S. Li and R. D. Murch, "An investigation into baseband techniques for communication systems," *IEEE Trans. Wirel. Commun.*, vol. 13, no. 9, pp. 4794–4806, Sep. 2014.
- [27] D. Korpi, L. Anttila, V. Syrjälä, and M. Valkama, "Widely linear digital self-interference cancellation in direct-conversion full-duplex transceiver," *IEEE J. Sel. Areas Commun.*, vol. 32, no. 9, pp. 1674–1687, Sep. 2014.
- [28] S. Javidi, M. Pedzisz, S. L. Goh, and D. P. Mandic, "The augmented complex least mean square algorithm with application to adaptive prediction problems," in *Proc. 1st IARP Workshop Cogn. Inform. Process.*, Jun. 2008, pp. 54–57.
- [29] Y. Xia, S. C. Douglas, and D. P. Mandic, "Adaptive frequency estimation in smart grid applications: Exploiting noncircularity and widely linear adaptive estimators," *IEEE Signal Process. Mag.*, vol. 29, no. 5, pp. 44–54, Sep. 2012.
- [30] Y. Xia and D. P. Mandic, "Widely linear adaptive frequency estimation of unbalanced three-phase power systems," *IEEE Trans. Instrum. Meas.*, vol. 61, no. 1, pp. 74–83, Jan. 2012.
- [31] M. Sakai, H. Lin, and K. Yamashita, "Self-interference cancellation in full-duplex wireless with IQ imbalance," *Phys. Commun.*, vol. 18, pp. 2–14, Dec. 2016.
- [32] A. A. Abidi, "Direct-conversion radio transceivers for digital communications," *IEEE J. Solid-State Circuits*, vol. 30, no. 12, pp. 1399–1410, Dec. 1995.
- [33] L. Anttila, M. Valkama, and M. Renfors, "Circularity-based I/Q imbalance compensation in wideband direct-conversion receivers," *IEEE Trans. Veh. Technol.*, vol. 57, no. 4, pp. 2099–2113, Jul. 2008.
- [34] B. Picinbono and P. Chevalier, "Widely linear estimation with complex data," *IEEE Trans. Signal Process.*, vol. 43, no. 8, pp. 2030–2033, Aug. 1995.
- [35] B. Picinbono and P. Bondon, "Second-order statistics of complex signals," *IEEE Trans. Signal Process.*, vol. 45, no. 2, pp. 411–420, Feb. 1997.
- [36] K. M. Gharaibeh, *Nonlinear Distortion in Wireless Systems: Modeling and Simulation with MATLAB*. John Wiley & Sons, 2011.
- [37] S. Wei, D. L. Goeckel, and P. A. Kelly, "Convergence of the complex envelope of bandlimited OFDM signals," *IEEE Trans. Inf. Theory*, vol. 56, no. 10, pp. 4893–4904, Oct. 2010.
- [38] 3GPP Technical Specification Group Radio Access Network, *LTE physical layer - General description*, TR 36.201, Nov. 2007.
- [39] D. P. Mandic and S. L. Goh, *Complex Valued Nonlinear Adaptive Filters: Noncircularity, Widely Linear and Neural Models*. John Wiley & Sons, 2009.
- [40] B. Fisher and N. J. Bershad, "The complex LMS adaptive algorithm-Transient weight mean and covariance with application to the ALE," *IEEE Trans. Acoust., Speech, Signal Process.*, vol. ASSP-31, no. 1, pp. 34–44, Feb. 1983.
- [41] D. P. Mandic, S. Kanna, and S. C. Douglas, "Mean square analysis of the CLMS and ACLMS for non-circular signals: The approximate uncorrelating transform approach," in *Proc. IEEE Int. Conf. Acoust., Speech, Signal Process. (ICASSP)*, Mar. 2015, pp. 3531–3535.
- [42] Y. Xia and D. Mandic, "Complementary mean square analysis of augmented CLMS for second order noncircular Gaussian signals," *IEEE Signal Process. Lett.*, vol. 24, no. 9, pp. 1413–1417, Sep. 2017.
- [43] —, "A full mean square analysis of CLMS for second-order noncircular inputs," *IEEE Trans. Signal Process.*, vol. 65, no. 21, pp. 5578–5590, Nov. 2017.
- [44] S. C. Douglas and D. P. Mandic, "Performance analysis of the conventional complex LMS and augmented complex LMS algorithms," in *Proc. IEEE Int. Conf. Acoust., Speech, Signal Process. (ICASSP)*, Mar. 2010, pp. 3794–3797.
- [45] D. P. Mandic, Y. Xia, and S. C. Douglas, "Steady state analysis of the CLMS and augmented CLMS algorithms for noncircular complex signals," in *Proc. 44th Asilomar Conf. on Signals, Syst. Comput. (ASILOMAR)*, Nov. 2010, pp. 1635–1639.
- [46] A. Feuer and E. Weinstein, "Convergence analysis of LMS filters with uncorrelated Gaussian data," *IEEE Trans. Acoust.*, vol. 33, no. 1, pp. 222–230, Feb. 1985.
- [47] T. Y. Al-Naffouri and A. H. Sayed, "Transient analysis of adaptive filters with error nonlinearities," *IEEE Trans. on Signal Process.*, vol. 51, no. 3, pp. 653–663, Mar. 2003.
- [48] —, "Transient analysis of data-normalized adaptive filters," *IEEE Trans. Signal Process.*, vol. 51, no. 3, pp. 639–652, Mar. 2003.
- [49] A. H. Sayed, *Adaptive Filters*. John Wiley & Sons, 2011.